Numerical Simulation of the 2D Non-Parabolic MEP Energy-Transport Model with a Mixed Finite Elements Scheme

Americo Marrocco, V. Romano, J.M. Sellier

INRIA

INSTITUT NATIONAL DE RECHERCHE EN INFORMATIQUE ET EN AUTOMATIQUE

Numerical Simulation of the 2D Non-Parabolic MEP Energy-Transport Model with a Mixed Finite Elements Scheme

A. Marrocco and V. Romano and J.M. Sellier

N° 5103

Février 2004

THÈME 4

ISSN 0249-6399 ISRN INRIA/RR--5103--FR+ENG

INRIA
ROCQUENCOURT

Numerical Simulation of the 2D Non-Parabolic MEP Energy-Transport Model with a Mixed Finite Elements Scheme

A. Marrocco* and V. Romano† and J.M. Sellier‡*

Thème 4 — Simulation et optimisation
de systèmes complexes
Projet Bang

Rapport de recherche n° 5103 — Février 2004 — 33 pages

Abstract: In [1] the Mixed Finite Element approximation scheme has been used to simulate a consistent hydrodynamical model for electron transport in semiconductors, free of any fitting parameters [3, 4, 5], based on the Maximum Entropy Principle (MEP) and assuming the Parabolic Band approximation. In this paper we describe an application of the above numerical method in the case of the two dimensional Non-Parabolic MEP energy-transport model. We can consider this paper as a generalization of what has been done in [1]. As done in [1] results of the simulation of 2D-MESFET and 2D-MOSFET Silicon devices are presented.

Key-words: numerical simulation, mixed finite element, MESFET and MOSFET semiconductor devices, maximum entropy principle, Kane's model for energy band, automatic differentiation

* Inria, Domaine de Voluceau, Rocquencourt BP 105 78153 Le Chesnay, France
† Facoltà di Ingegneria sede di Enna, Dipartimento di Matematica e Informatica, Università di Catania, Viale A.Doria 6, I-95125 Catania, Italy
‡ Dipartimento di Matematica e Informatica, Università di Catania, Viale A. Doria 6, I-95125 Catania, Italy

Unité de recherche INRIA Rocquencourt
Domaine de Voluceau, Rocquencourt, BP 105, 78153 Le Chesnay Cedex (France)
Téléphone : +33 1 39 63 55 11 — Télécopie : +33 1 39 63 53 30

Simulation numérique par éléments finis mixtes d'un modèle Energy-Transport formulé à l'aide du principe d'entropie maximum et utilisant une approximation non-parabolique des bandes d'énergie

Résumé : Dans [1] nous avons utilisé une approche éléments finis mixtes pour la simulation numérique d'un modèle hydrodynamique consistant, décrivant le transport d'électrons dans des matériaux semi-conducteurs (Si). Ce modèle, exempt de toute approximation de paramètres physiques, est basé sur le principe d'entropie maximum (MEP) et dans la référence citée plus haut nous avons considéré l'approximation parabolique classique des bandes d'énergie.

Dans le présent rapport, on étend le schéma numérique au cas de l'approximation non-parabolique des bandes d'énergie (cas des relations de dispersion de Kane). Des résultats numériques pour les dispositifs déjà utilisés dans [1] sont présentés.

Mots-clés : simulation numérique, éléments finis mixtes, dispositifs semi-conducteurs MESFET et MOSFET, principe d'entropie maximum, approximation de Kane pour les bandes d'énergie, différentiation automatique

1 Introduction

In the nowaday submicron Silicon devices, the miniaturization is very advanced. Due to the tremendous decreasing of the characteristic dimensions of semiconductor devices, models like the well-know Drift-Diffusion are not apprpriate for the simulation of carrier transport in such a devices. However, the energy transport models which are implemented in commercial simulators are based on phenomenological constitutive equations for the particle flux and energy flux depending on a set of parameters which are fitted to homogeneous bulk material Monte Carlo simulations. However, a more satisfactory physical description should be based on relating the parameters appearing in the constitutive laws to the fundamental scattering properties of electrons with phonons and impurities [7]. That is why in a precedent paper [1], motived by the need of accurate simulations of the carrier transport in such a submicron Silicon semiconductors devices and the need of non-dependence from any fitting parameters, we have presented simulation results of various 2D Silicon devices (i.e. MESFET and MOSFET), based on a consistent energy-transport model, free of any fitting parameters [3, 4, 5] recovered from the Maximum Entropy Principle (MEP). That model take into account all the relevant scattering mechanism in Silicon, e.g. scattering of electrons with acoustic and non-polar phonons and with impurities and assume as energy band the Parabolic band approximation. In [5], it has been shown that it is possible to recover an energy-transport limiting model which is equivalent in the stationary case to the original one (Hydrodynamical model), at least for smooth solutions and in the case of the Non-Parabolic band approximation (Kane dispersion relation).

In the present paper we use the energy-transport formulation of the model for simulating the steady state of a 2D-MESFET and a 2D-MOSFET silicon device in the Kane dispersion relation case.

As in [1] the numerical scheme is based on mixed finite elements which guarantee accurate current conservation and allow to deal also with very complex geometry domains. For the theoretical details of the scheme the interested reader is referred to [2, 8, 9]. As said in [1] the above method guarantees a very good numerical current conservation and is very stable and robust.

2 The MEP energy-transport model in the Kane dipersion relation case

In this section we give only a brief sketch of the Energy-Transport model which we will use. We limit our discussion to the case of Kane dipersion relation.

It is assumed that the conduction band is described around each minimum (valley) by the Kane dispersion relation approximation

$$\mathcal{E}(\mathbf{k})\big[1+\alpha\mathcal{E}(\mathbf{k})\big] = \frac{\hbar^2 k^2}{2m^*}, \qquad \mathbf{k}\in\mathbf{R^3}\,, \tag{1}$$

where $\mathcal{E}$ is the electron energy, m^* is the effective electron mass (which is 0.32 m_e in Silicon, with m_e the electron mass in the vacuum), $\hbar\mathbf{k}$ is the crystal momentum, $\hbar$, as usual, the Planck constant divided by 2π and α is the non-parabolicity factor ($\alpha = 0.5eV^{-1}$ for Silicon). Obviously, in the case of $\alpha = 0$ we obtain the parabolic energy band.

The energy-transport model obtained for silicon semiconductor in [5, 6], starting from the hydrodynamical model based on the maximum entropy principle [3, 4], is given by the following set of balance equations for the electron density n and energy W, coupled to the Poisson equation for the electric potential ϕ

$$\frac{\partial n}{\partial t} + \mathrm{div}(n\mathbf{V}) = 0, \tag{2}$$

$$\frac{\partial (nW)}{\partial t} + \mathrm{div}(n\mathbf{S}) - ne\mathbf{V}\cdot\nabla\phi = nC_W, \tag{3}$$

$$\epsilon\Delta\phi = -e(N_D - N_A - n)\,, \tag{4}$$

where N_D and N_A are the donor and acceptor densities respectively, e is the elementary charge, ϵ is the dielectric constant while div, ∇ and Δ are the divergence, gradient and laplacian operators.

The evolution equations are closed with the constitutive relations for the velocity $\mathbf{V}$ and the energy-flux $\mathbf{S}$

$$\mathbf{V} = D_{11}(W)\nabla\log n + D_{12}(W)\nabla W + D_{13}(W)\nabla\phi, \tag{5}$$

$$\mathbf{S} = D_{21}(W)\nabla\log n + D_{22}(W)\nabla W + D_{23}(W)\nabla\phi. \tag{6}$$

The elements of the diffusion matrix $D = (D_{ij})$ read

$$D_{11} = \frac{c_{22}U^{(0)} - c_{12}F^{(0)}}{c_{11}c_{22} - c_{12}c_{21}}, \quad D_{12} = \frac{c_{22}U^{(0)\prime} - c_{12}F^{(0)\prime}}{c_{11}c_{22} - c_{12}c_{21}},$$

$$D_{13} = -e\frac{c_{22} - c_{12}G^{(0)}}{c_{11}c_{22} - c_{12}c_{21}},$$

$$D_{21} = \frac{c_{11}F^{(0)} - c_{21}U^{(0)}}{c_{11}c_{22} - c_{12}c_{21}}, \quad D_{22} = \frac{c_{11}F^{(0)\prime} - c_{21}U^{(0)\prime}}{c_{11}c_{22} - c_{12}c_{21}},$$

$$D_{23} = e\frac{c_{21} - c_{11}G^{(0)}}{c_{11}c_{22} - c_{12}c_{21}}.$$

All the coefficients c_{ij} and the functions $U^{(0)}$, $F^{(0)}$, $G^{(0)}$ depend on the energy W. The prime denotes derivative with respect to W.

The energy production term has a relaxation form $C_W = -\frac{W-W_0}{\tau_W}$ where τ_W is the energy relaxation time, which depends also on W, and $W_0 = 3/2k_BT_L$ is the energy at equilibrium, with T_L the lattice temperature, here assumed to be constant.

The expressions of $U^{(0)}$, $F^{(0)}$,$G^{(0)}$, τ_W, c_{ij}, D_{ij} have been obtained in [3, 4] both for parabolic band and Kane's dispersion relation.

However in the case when the conduction energy bands of electrons are described by the Kane dispersion relation, the expressions of $U^{(0)}$, $F^{(0)}$,$G^{(0)}$ τ_W, c_{ij}, require a numerical evaluation of some integrals and for them an analytical expression is not available. These computations have been done in [3, 4] and, in order to improve the efficiency of the simulation code, discrete data have been approached by splines.

MESFET devices are unipolar. On the contrary, MOSFET devices are bipolar and therefore we need a transport model for the holes. Here we assume that the contribution of holes to the total current is a secondary effect and thus it suffices to use a drift-diffusion model. It reads:

$$\frac{\partial p}{\partial t} + \nabla\cdot\mathbf{J_p} = 0 \tag{7}$$

$$\mathbf{J_p} = -\mu_p p \nabla\phi - D_p \nabla p \tag{8}$$

where p is the hole density, $\mathbf{J_p}$ is the hole particle flux, μ_p the hole mobility and D_p the diffusivity. In the bipolar case the Poisson equation must include both densities of electrons and holes and reads

$$\mathbf{E} = -\nabla\phi, \qquad \nabla\cdot(\epsilon\nabla\phi) = -e(N_D - N_A - n + p) \tag{9}$$

In order to use the numerical method we will show in the following sections, the MEP Energy-Transport model must be formulated in an equivalent form. This is done in the next section.

3 Formulation of the model in the framework of linear irreversible thermodynamics

We start briefly recalling the basic formulation of linear irreversible thermodynamics. Let $s_n = s_n(u_n, n)$ be the electron system entropy density (where u_n is the electron energy density and n the electron density) and T_n the electron temperature (the lattice and the electron system are assumed to be at different temperature). The first principle of thermodynamics gives:

$$T_n ds_n = du_n - \nu_n dn\,, \tag{10}$$

where ν_n can be interpreted as the chemical potential and reads

$$\nu_n = e(\varphi_n + \phi)\,, \tag{11}$$

where ϕ is the electrostatic potential. It is convenient to introduce the electrochemical potential $\hat{\phi}_n$ by the following definition

$$\hat{\phi}_n = -\nu_n + e\phi\,. \tag{12}$$

In standard irreversible thermodynamics [16] the entropy fluxes $\mathcal{J}_L^s$ of the lattice and of the electron system $\mathcal{J}_n^s$ are related to the particle and energy fluxes by the following relationships:

$$\mathcal{J}_{\mathbf{L}}^{\mathbf{s}} = \frac{\mathcal{J}_{\mathbf{L}}^{\mathbf{u}}}{T_L}, \quad \mathcal{J}_{\mathbf{n}}^{\mathbf{s}} = \frac{\mathcal{J}_{\mathbf{n}}^{\mathbf{u}} - \nu_n \mathcal{J}_{\mathbf{n}}}{T_N}\,, \tag{13}$$

where $\mathcal{J}_{\mathbf{L}}^{\mathbf{u}}$ and $\mathcal{J}_{\mathbf{n}}^{\mathbf{u}}$ are the lattice and electron energy flux respectively, $\mathcal{J}_{\mathbf{n}} = n\mathbf{V}$ the electron particle flux, T_L and T_n the lattice and electron gas temperature respectively. Now, according to the tenets of linear irreversible thermodynamics [16] the thermodynamic forces are linearly related to the thermodynamic fluxes as follows:

$$\mathcal{J}_{\mathbf{n}} = \frac{L_{11}}{T_n}\nabla\hat{\phi}_n + L_{12}\nabla\frac{1}{T_n}, \tag{14}$$

$$T_n\mathcal{J}_{\mathbf{n}}^{\mathbf{s}} = \frac{L_{21}}{T_n}\nabla\hat{\phi}_n + L_{22}\nabla\frac{1}{T_n}\,, \tag{15}$$

where the matrix L_{ij} is symmetric if, and only if, the Onsager reciprocity relations hold. In terms of electron energy flux $\mathcal{J}_{\mathbf{u}}^{\mathbf{s}}$ we rewrite the above equations as

$$\mathcal{J}_{\mathbf{n}} = \frac{L_{11}}{T_n}\nabla\hat{\phi}_n + L_{12}\nabla\frac{1}{T_n}, \tag{16}$$

$$\mathcal{J}_{\mathbf{n}}^{\mathbf{u}} = \big(\nu_n\frac{L_{11}}{T_n} + \frac{L_{21}}{T_n}\big)\nabla\hat{\phi}_n + (\nu_n L_{12} + L_{22})\nabla\frac{1}{T_n}\,. \tag{17}$$

Now, for the electron system, described by a probability density function f, the entropy density in the maxwellian limit of the Fermi-Dirac statistics is defined as

$$s_n = -k_B \int_B (f \log f - f) d^3\mathbf{k} \,, \tag{18}$$

where $\mathbf{k}$ is the electron wave-vector which belongs to the first Brillouin zone. This latter both in the parabolic and non-parabolic band approximation is extended to all $\mathbf{R^3}$.

By introducing the function

$$\eta(f) = -k_B(f \log f - f) \,,$$

we can write the electronic entropy s_n as

$$s_n = \int_B \eta(f) d^3\mathbf{k} \,. \tag{19}$$

As shown in [3, 4], the zeroth order maximum entropy distribution function is

$$f_{ME} = \exp\left(-\frac{\lambda}{k_B} - \lambda^W \mathcal{E}\right) \,, \tag{20}$$

where λ,λ^W are the Langrange multipliers relative to the density and energy. It easily follows that

$$\eta(f_{ME}) = k_B f_{ME} \left(1 + \frac{\lambda}{k_B} + \lambda^W \mathcal{E}\right). \tag{21}$$

Since

$$df_{ME} = -f_{ME} \left(\frac{d\lambda}{k_B} + \mathcal{E} d\lambda^W\right) \,, \tag{22}$$

it also follows that

$$d\eta = -f_{ME} \left[\left(\frac{\lambda}{k_B} + \mathcal{E}\lambda^W\right)(d\lambda + k_B \mathcal{E} d\lambda^W)\right] \,. \tag{23}$$

Consequently, for the differential of the entropy density, ds_n, we have

$$ds_n = \int_B d\eta d^3\mathbf{k} = -\frac{\lambda}{k_B} n d\lambda - d(\lambda\lambda^W) u_n - k_B \lambda^W d\lambda^W Z \,, \tag{24}$$

where n is the electron particle density calculated with the zeroth order f_{ME} distribution function, which reads

$$n = \int_B f_{ME} d^3\mathbf{k} \,. \tag{25}$$

Likewise u_n is the electron energy density calculated with the zeroth order f_{ME} distribution function and reads

$$u_n = nW = \int_B \mathcal{E} f_{ME} d^3\mathbf{k} \,,$$

while Z is the quantity

$$Z = \int_B \mathcal{E}^2 f_{ME} d^3\mathbf{k}.$$

From the definition of n, substituting (22) in the differential of (25) , we have

$$dn = -n\frac{d\lambda}{k_B} - d\lambda^W u_n \,. \tag{26}$$

Likewise, from the definition of u_n we get

$$du_n = -u_n\frac{d\lambda}{k_B} - d\lambda^W Z \,. \tag{27}$$

Now, from (24),(26) and (27), we easily get

$$ds_n = \lambda dn + k_B\lambda^W du_n \,, \tag{28}$$

which has the same form as equation (10) provided the following identifications are made

$$k_B\lambda^W = \frac{1}{T_n}, \quad \nu_n = -\lambda T_n \,. \tag{29}$$

Therefore, until now, we have proved that the expression for the entropy differential as obtained from the maximum entropy ansatz can be written in the form of linear irreversible thermodynamics.

Now, it is easy to see that, in terms of $W = \frac{u_n}{n}$, the energy per particle, we can write equation (26) as

$$\frac{dn}{n} = -\frac{d\lambda}{k_B} - W d\lambda^W \,. \tag{30}$$

Then introducing the primitive (defined up to a constant)

$$F(W) = \int W\frac{d\lambda^W}{dW}dW \,,$$

and integrating (30) we obtain

$$\lambda = -k_B \log n - k_B F(W) \,, \tag{31}$$

which, after substituting into the equation $(29)_2$, yields

$$\nu_n = k_B T_n \log n + k_B T_n F(W), \tag{32}$$

$$d\nu_n = k_B T_n d\log n + \big(k_B \log n + k_B F - \frac{W}{T_n}\big)dT_n \,, \tag{33}$$

where the equation (33) has been obtained by differentiating equation (32).

Substituting (32), (33) and (12) into equations (16),(17) yields

$$\mathcal{J}_\mathbf{n} = -L_{11}k_B\nabla\log n + \frac{qL_{11}}{T_n}\nabla\phi - \left[\frac{L_{11}}{T_n}\left(k_B\log n + k_B F - \frac{W}{T_n}\right) + \frac{L_{12}}{T_n^2}\right]\nabla T_n \,, \tag{34}$$

$$\mathcal{J}^\mathbf{u}_\mathbf{n} = -(\nu_n L_{11} + L_{21})k_B\nabla\log n + (\nu_n L_{11} + L_{21})\frac{e}{T_n}\nabla\phi - \tag{35}$$

$$\left[\left(\frac{\nu_n L_{11} + L_{21}}{T_n}\right)\left(k_B\log n + k_B F - \frac{W}{T_n}\right) + \left(\frac{\nu_n L_{12} + L_{22}}{T_n^2}\right)\right]\nabla T_n \,. \tag{36}$$

By comparing these last two equations with the maximum entropy derived constitutive equations for the energy transport model (5)-(6) we have the following identification

$$D_{11} = -\frac{k_B L_{11}}{n}, \quad D_{13} = \frac{eL_{11}}{nT_n}, \tag{37}$$

$$D_{12} = -\frac{1}{n}\left[\frac{L_{11}}{T_n}\left(k_B \log n + k_B F - \frac{W}{T_n}\right) + \frac{L_{12}}{T_n^2}\right]\frac{dT_n}{dW}, \tag{38}$$

$$D_{21} = -\frac{k_B(\nu_n L_{11} + L_{21})}{n}, \quad D_{23} = e\frac{\nu_n L_{11} + L_{21}}{nT_n}, \tag{39}$$

$$D_{22} = -\frac{1}{n}\left[\frac{\nu_n L_{11} + L_{21}}{T_n}\left(k_B \log n + k_B F - \frac{W}{T_n}\right) + \frac{\nu_n L_{12} + L_{22}}{T_n^2}\right]\frac{dT_n}{dW}, \tag{40}$$

which can be considered a system in the unknowns L_{ij}. After some standard algebra, we get

$$L_{11} = -\frac{nD_{11}}{k_B}, \tag{41}$$

$$L_{12} = +\frac{nD_{12}}{k_B\frac{d\lambda^W}{dW}} + \frac{nD_{11}}{k_B}(\nu_n - W), \tag{42}$$

$$L_{21} = -\frac{nD_{21}}{k_B} + \frac{nD_{11}}{k_B}\nu_n, \tag{43}$$

$$L_{22} = +\frac{nD_{22}}{k_B\frac{d\lambda^W}{dW}} + \frac{nD_{11}}{k_B}\nu_n(\nu_n - W) - L_{12}\left[(\nu_n - W) + \nu_n\right], \tag{44}$$

where we have used the following results

$$\log n + F = \nu_n \lambda^W, \quad \frac{W}{T_n} = W\lambda^W k_B,$$

with

$$N_c = 2\left(\frac{2\pi k_B m^* T_n}{\hbar^2}\right)^{\frac{3}{2}}, \quad n = N_c(T_n)\exp\left(e\frac{\phi + \varphi_n}{k_B T_n}\right),$$

where φ_n is the so-called electron quasi-Fermi level. It is very important to note that the solution (41)-(44) is not the only one possible because actually the system (37)-(40) is a system of *6 equations in only 4 unknowns*. However, it is very easy to show, in both the parabolic band and Kane-band approximations, that the solutions for L_{11} and L_{21}

$$L_{11} = -\frac{nD_{11}}{k_B}, \quad L_{21} = \frac{-n(D_{12} + \nu_n D_{11})}{k_B},$$

and

$$L_{11} = \frac{nD_{13}}{e}T_n, \quad L_{21} = \frac{nD_{23}T_n}{e} - \nu_n L_{11},$$

are theoretically equivalent.
At this point we want to transform, in the stationary case, the system (2)-(4) in the following

form

$$-\text{div } \mathbf{J_n} = 0, \tag{45}$$

$$-\text{div } \mathbf{J_n^T} + n\frac{W - W_0}{\tau_W} = 0, \tag{46}$$

$$\text{div } \mathbf{D} = e(N_D - N_A - n + p), \tag{47}$$

$$\mathbf{J_n} = A_{11}\nabla\left(\frac{\varphi_n}{T_n}\right) + A_{12}\nabla\left(\frac{-1}{T_n}\right), \tag{48}$$

$$\mathbf{J_n^T} = A_{21}\nabla\left(\frac{\varphi_n}{T_n}\right) + A_{22}\nabla\left(\frac{-1}{T_n}\right), \tag{49}$$

where $\mathbf{D}$ is the electric displacement vector and we denote, now, with $\mathbf{J_n}$ the electron current $-en\mathcal{J}_\mathbf{n}$. The generation-recombination effects have been neglected. In order to get the sought transformation we need to find the analytical expression of the coefficients A_{ij} as functions of the variables D_{ij}. Let us start by finding the coefficients A_{11} and A_{12}. First of all, we note that

$$\mathbf{J_n} = -en\mathbf{V} = -en\left[D_{11}\nabla \log n + D_{12}\nabla W + D_{13}\nabla\phi\right], \tag{50}$$

$$\nabla T_n = -\nabla\left(\frac{1}{T_n}\right)T_n^2, \tag{51}$$

$$\frac{\nabla\phi}{T_n} = \nabla\left(\frac{\phi}{T_n}\right) - \phi\nabla\left(\frac{1}{T_n}\right), \tag{52}$$

$$\nabla logn = \frac{1}{n}\nabla n = \frac{1}{n}\nabla\left[N_c(T_n)exp.\left(e\frac{\varphi_n + \phi}{k_B T_n}\right)\right]. \tag{53}$$

Now, comparing equations (50)-(53) to equations (48), we get the following results

$$A_{11} = e^2 L_{11}, \quad A_{12} = -e^2 L_{11}\phi - \frac{en}{k_B}\left\{D_{11}W - \frac{D_{12}}{\frac{d\lambda^W}{dW}}\right\}. \tag{54}$$

Likewise, noting that

$$\mathbf{J_n^T} = -\mathcal{J}_\mathbf{n}^\mathbf{u} - \phi\mathbf{J_n}, \tag{55}$$

we get

$$A_{21} = e^2 L_{11}\varphi_n + eL_{21}, \quad A_{22} = e^2 L_{11}\varphi_n^2 + e(L_{21} + L_{12})\varphi_n + L_{22}. \tag{56}$$

We note that the matrix A is not any longer symmetric in the case of non-parabolic energy band, at difference of the parabolic case in which the matrix A was forced to be symmetric (thanks to Onsager principle).

4 The Numerical Approach

The MEP energy-transport model given as in (45)-(49) has the same structure as the family of models studied in [8]. In the last reference, the diffusion matrix A which depends on parameters

β,c,γ, is given explicitly by

$$A_{11} = n\mu_n e T_n \,, \tag{57}$$

$$A_{12} = n\mu_n e T_n \left(\beta \frac{k_B T_n}{e} \gamma - \varphi_n + \chi \right) , \tag{58}$$

$$A_{21} = A_{12} \,, \tag{59}$$

$$A_{22} = n\mu_n e T_n \left[\left(\beta \frac{k_B T_n}{e} \gamma - \varphi_n + \chi \right)^2 + (\beta - c) \left(\frac{k_B T_n}{e} \right)^2 \right] , \tag{60}$$

and by an appropriate choice of the parameters, the Stratton Energy-Transport model or the Degond Energy-Transport model can be recovered as well as some simplified hydrodynamical models (SHD) [10, 14]. In a previous paper [1] the numerical scheme developped in [8] was adapted in order to take into account the expression of the diffusion matrix built from the MEP model. In this former paper the particular case of the "parabolic band approximation" was considered. In this context, only the parameters C_{ij} (for the definition of the D matrix (5),(6)) and the right hand side C_W term (3) needed to be smoothed by (cubic) splines and this, in order to be able to evaluate easily partial derivative of the diffusion matrix A with respect to the unknowns of the problem.
In the present paper, only the way in which the diffusion matrix A is obtained changes in comparison with the previous parabolic band implementation. In particular for the parabolic band approximation, the parameters were considered as functions of the electron temperature T_n, and let us recall that all the derivatives (with respect to the unknowns) were computed using a procedure similar to the one used in softwares devoted to "automatic differentiation of FORTRAN codes". Let us recall (again) that what we really need is to be able to evaluate at any given point the value of

$$\frac{\partial B_{ij}}{\partial v_k} \,,$$

where B_{ij} is the inverse of the diffusion matrix A_{ij} and v_k one of the "entropic" variables.
In the Kane approximation context, the situation is a little bit different: It is difficult to express the parameters data like the C_{ij} as functions of the electron temperature T_n. The natural way the C_{ij} and other parameters are obtained is as function of the electron energy W (an explicit analytical relation between W and T_n is not available). So in the "Kane context", the parameters

$$C_{ij}, \quad C_W, \quad U, \quad F, \quad G, \quad \lambda^W \,,$$

are considered as functions of the electron energy W and approximated via cubic splines. The figure 1 gives the C_{ij} as functions of the electron energy W, the discrete data points are marked on the sub-figures; the dotted lines represents the cubic splines approximation. For the given values, the relative error is less than 0.1%, and from the picture we can see that extrapolated values ($W > 0.6$ eV) may be reasonably good until $W = 0.8$ eV (due to the C_{12} term). On the figure 2 we have reported approximation for the parameters C_W, U, F, G. For the subfigures B, C, D the continuous lines represents the function for the parabolic band approximation. In addition we have to consider the $\lambda^W(W)$ function. In figure 3 (A,B) we have two views of the $\lambda^W(W)$ data and approximated by splines. This function is also represented in continuous line for the parabolic band approximation. The subfigure (bottom) represents the function $W(T_n)$ and again the continuous line is for the parabolic band approximation (i.e. $W = \frac{3}{2} k_B T_n$). This last function $W(T_n)$ is needed in the process of derivative evaluations.

A

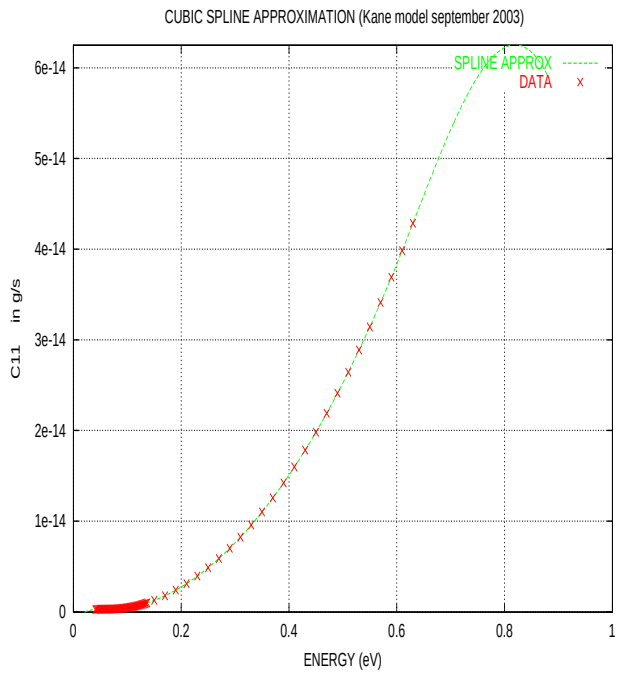

B

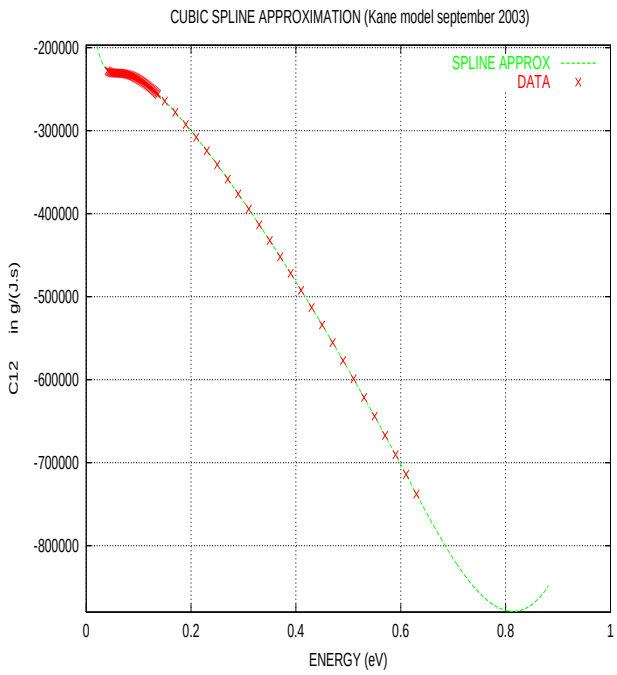

C

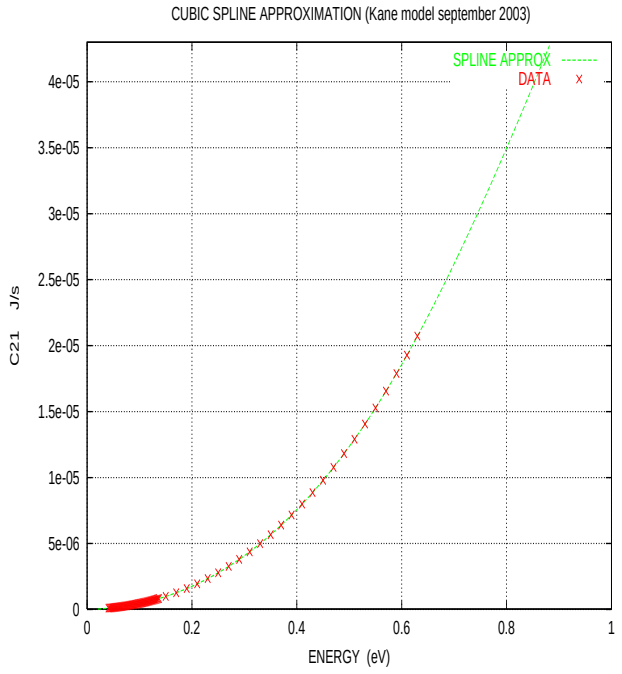

D

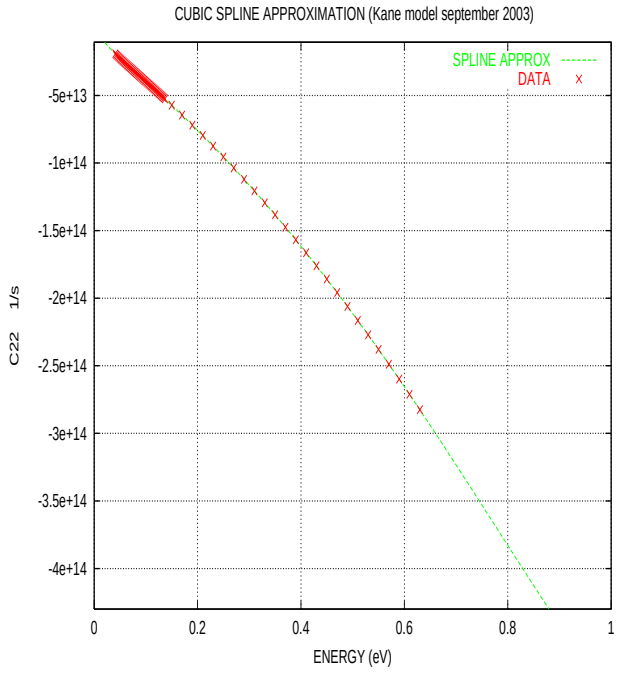

Figure 1: C_{ij} in the Kane approximation

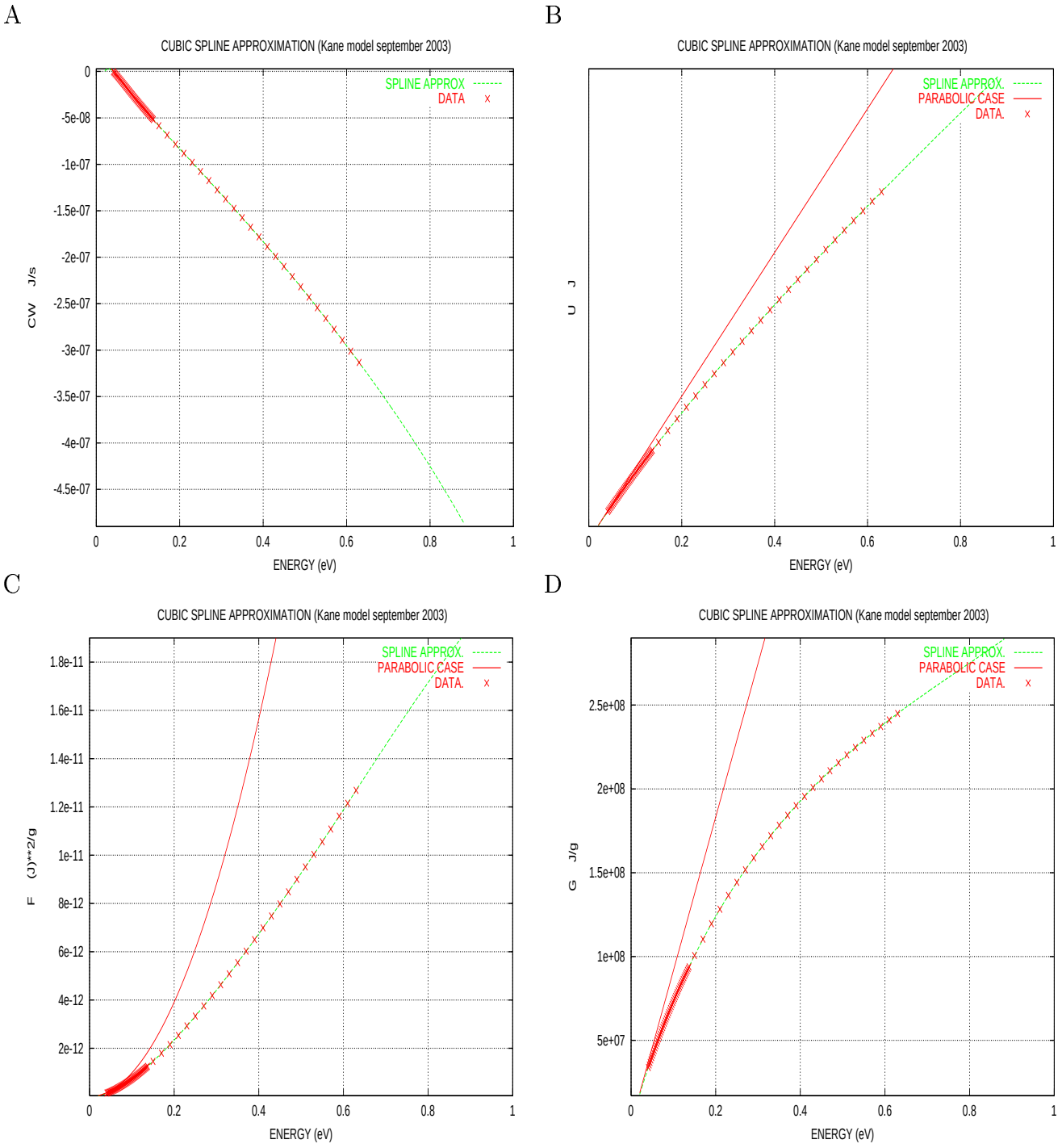

Figure 2: Other functions in the Kane approximation. The corresponding function in the parabolic band approximation is also given, when appropriate

A

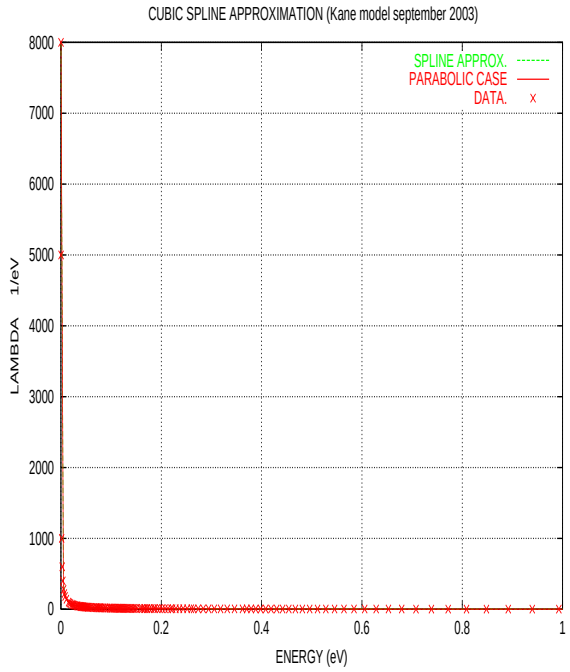

B

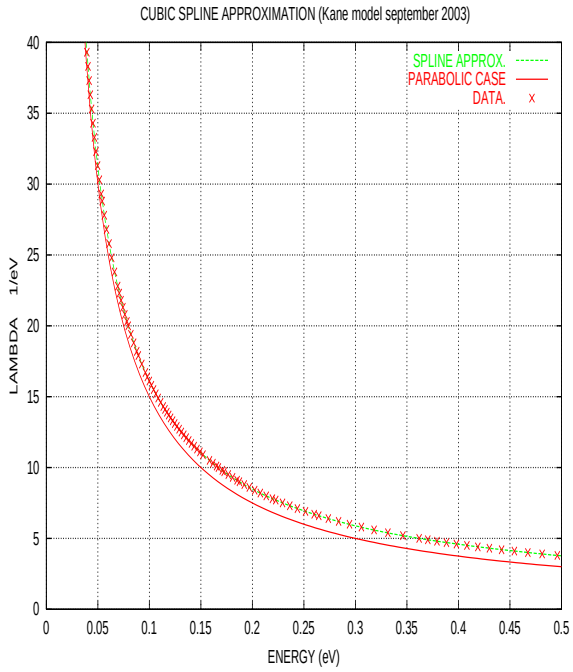

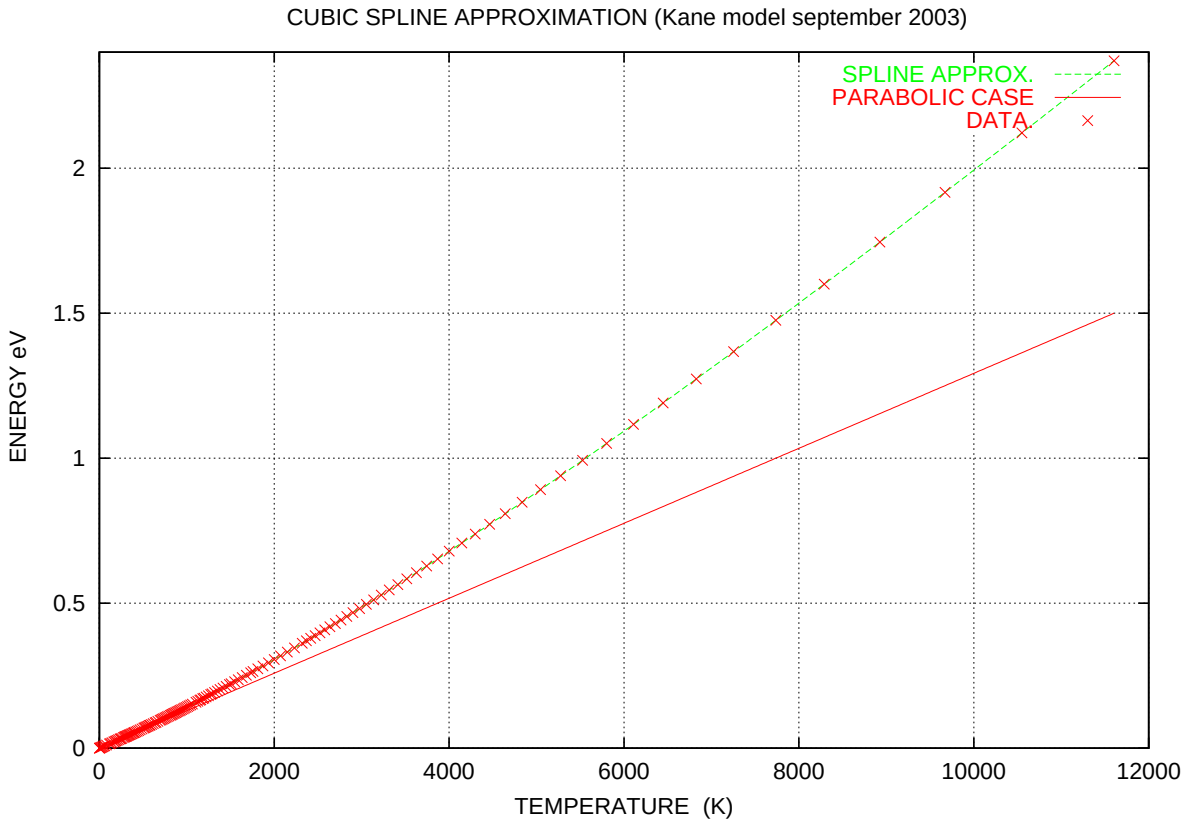

Figure 3: $\lambda(w)$ and $W(T_n)$ functions for the *Kane* and *Parabolic* band approximation models

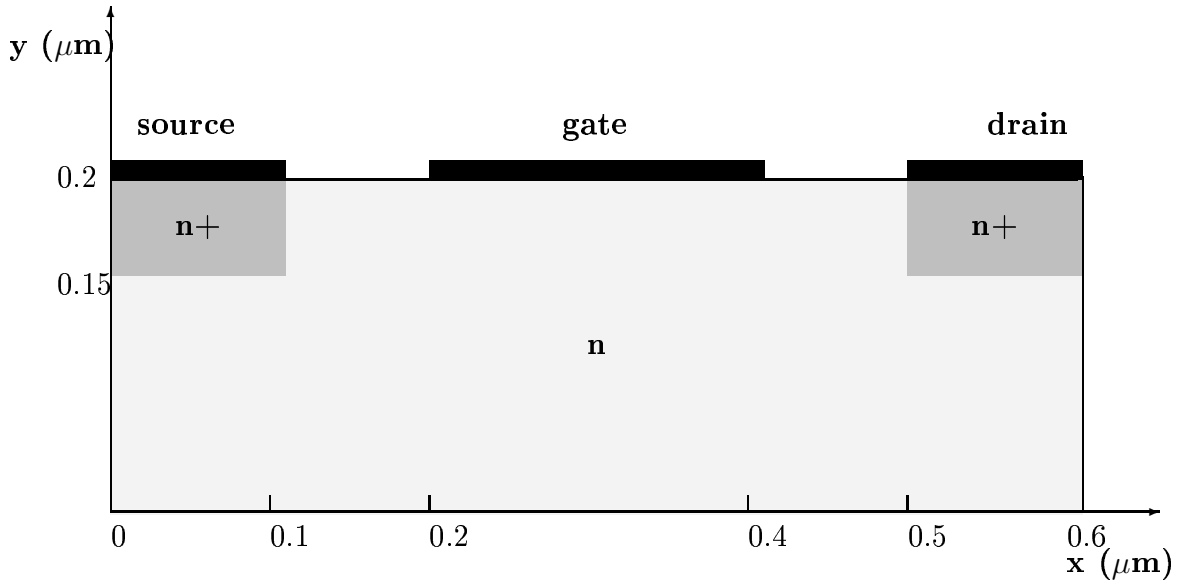

Figure 4: Schematic representation of a bidimensional MESFET

5 Simulation of a 2D silicon MESFET

In this section we check the validity and the efficiency of the numerical method by simulating a bidimensional Metal Semiconductor Field Effect Transistor (MESFET). The shape of the device is taken as rectangular and it is pictured in fig. 4.

The axes of the reference frame are chosen parallel to the edges of the device. We take the dimensions of the MESFET to be such that the numerical domain is

$$\Omega = [0, 0.6] \times [0, 0.2]$$

where the unit length is the micron.

The regions of high doping n^+ are the subset

$$[0, 0.1] \times [0.15, 0.2] \cup [0.5, 0.6] \times [0.15, 0.2].$$

The contacts at the source and drain are 0.1 μm wide and the contact at the gate is 0.2 μm wide. The distance between the gate and the other two contacts is 0.1 μm. The same doping concentration as in [21] is considered

$$n_D(x) - n_A(x) = \begin{cases} 3 \times 10^{17}\text{cm}^{-3} & \text{in the } n^+ \text{ regions} \\ 10^{17}\text{cm}^{-3} & \text{in the } n \text{ region} \end{cases}$$

with abrupt junctions.

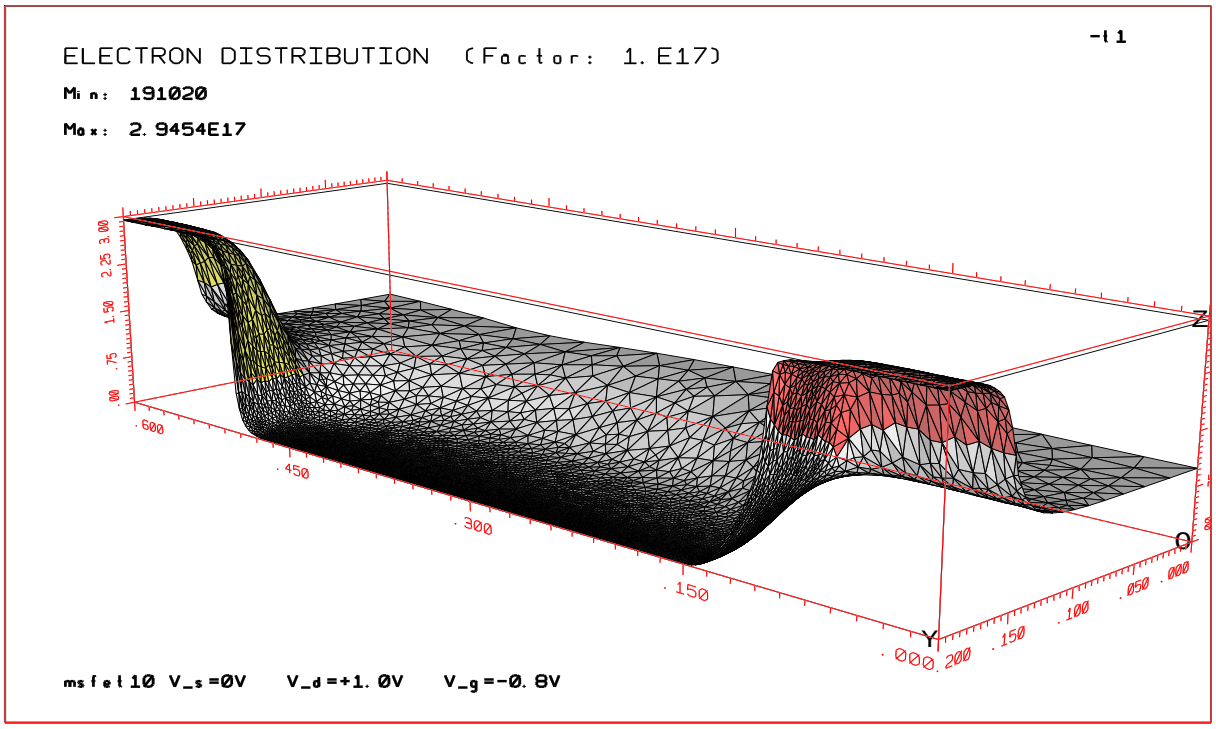

Figure 5: Stationary solution for the electron density in MESFET (cm^{-3}).

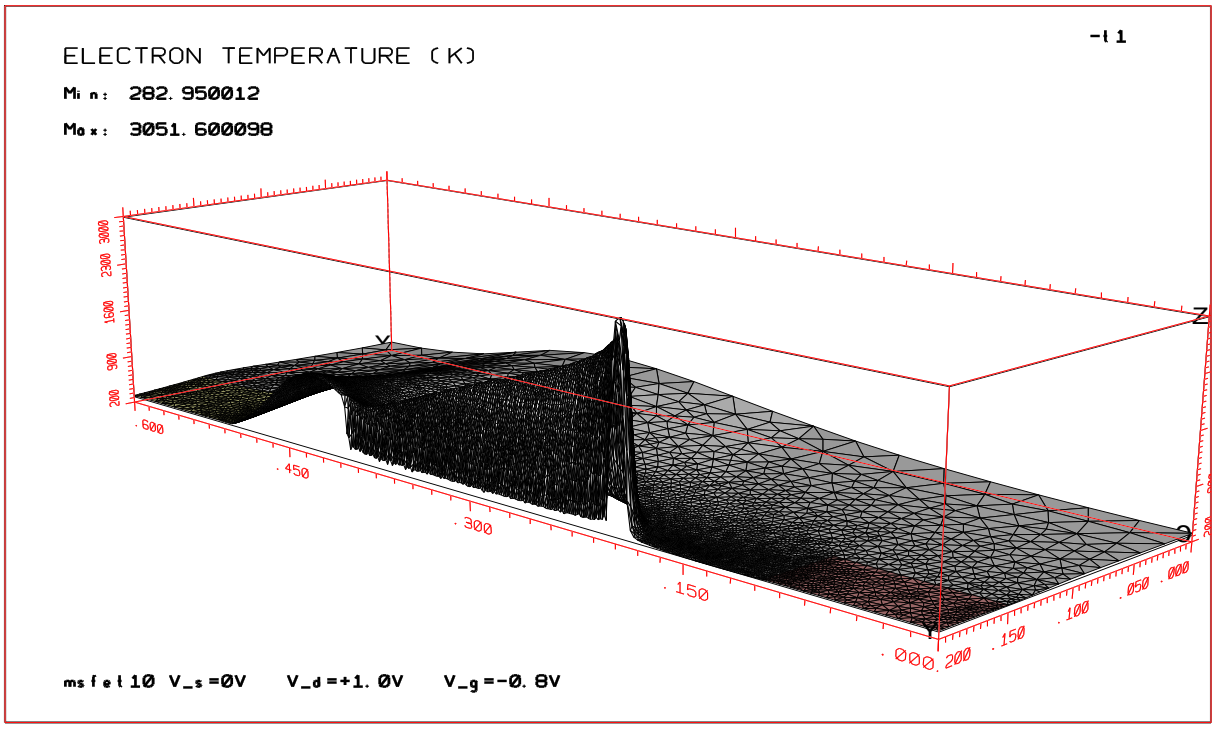

Figure 6: Stationary solution for the electron temperature in MESFET (K).

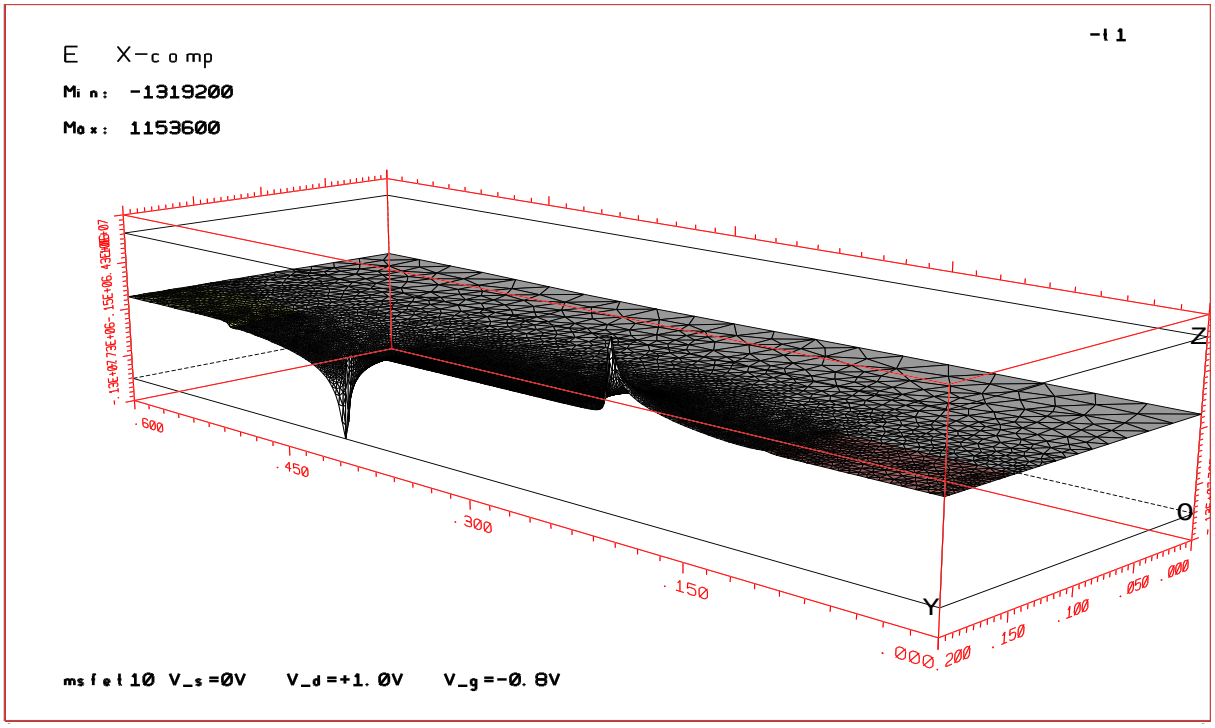

Figure 7: Stationary solution for the x-component of the electric field in MESFET (Volt/cm).

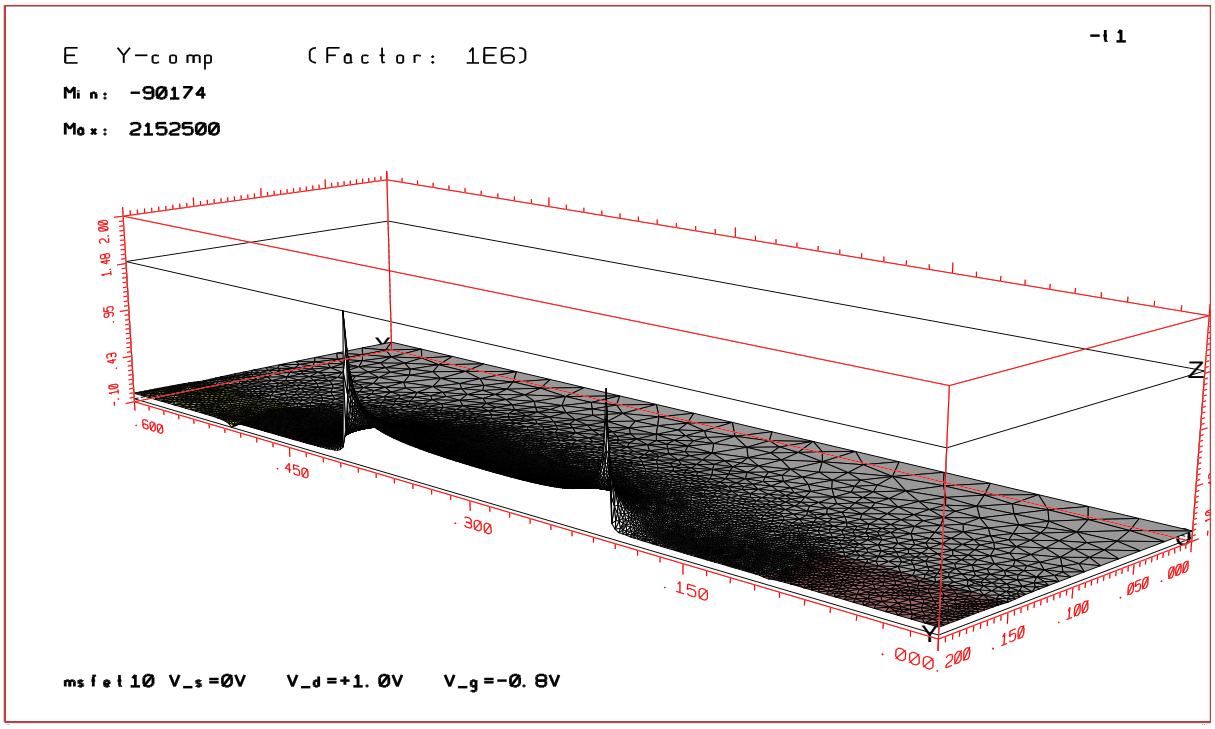

Figure 8: Stationary solution for the y-component of the electric field in MESFET (Volt/cm).

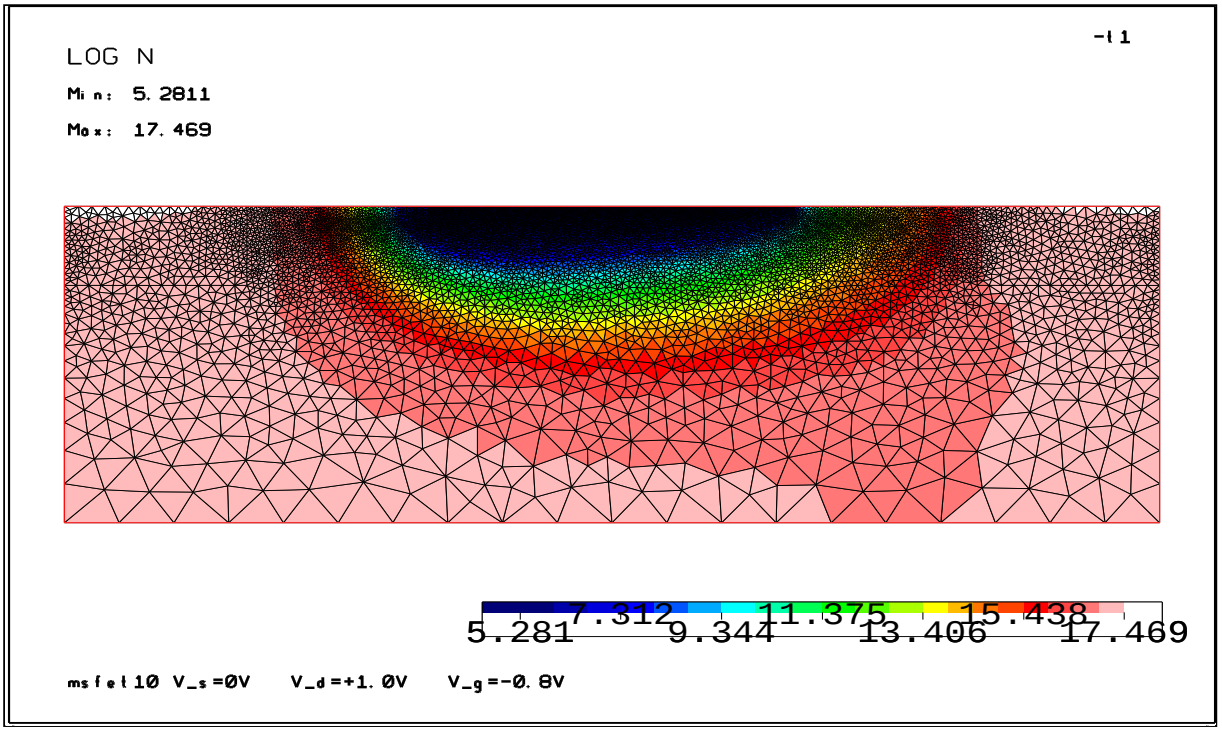

Figure 9: Distribution of electron carrier density (Log scale, contour plot).

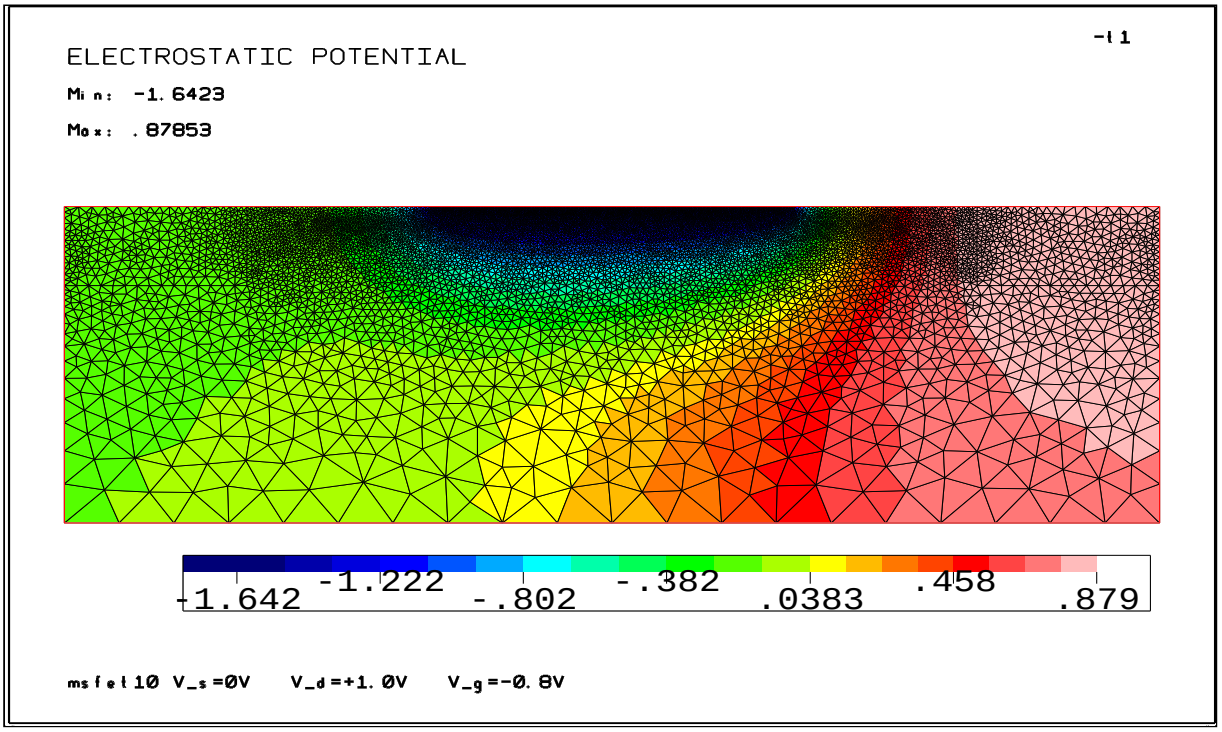

Figure 10: Electrostatic potential (contour plot).

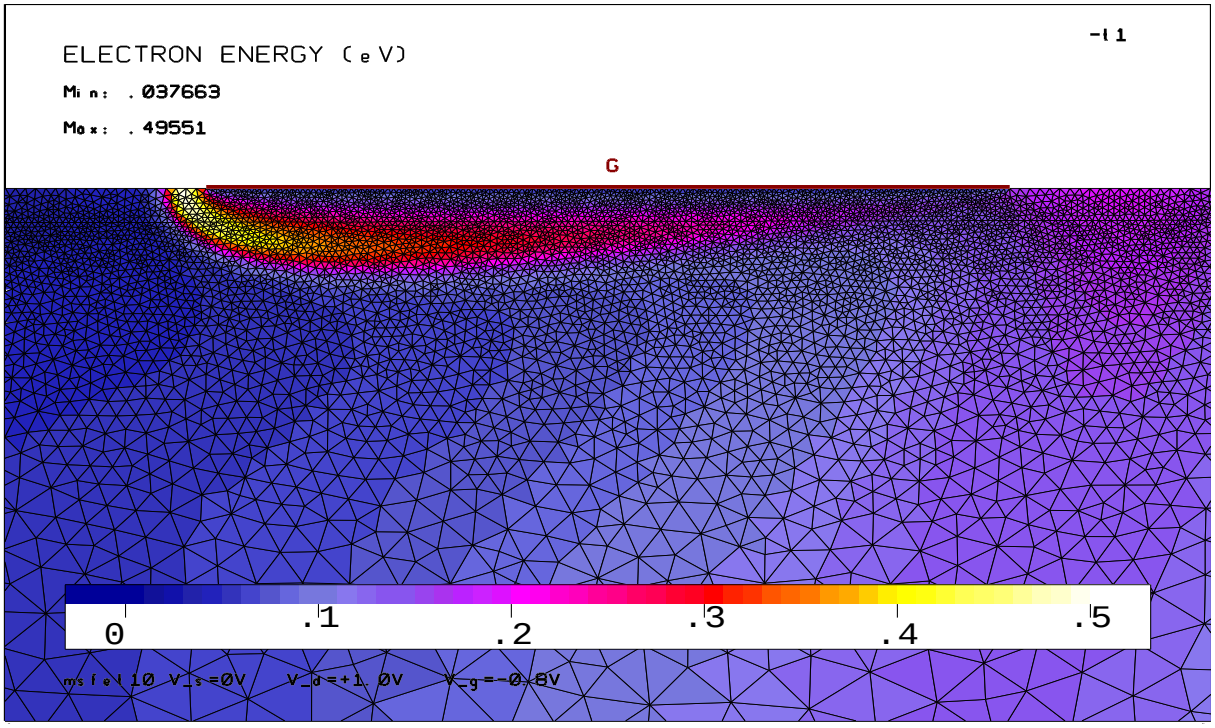

Figure 11: Distribution of electron energy for $V_G = -0.8V$ (contour plot, Zoom view).

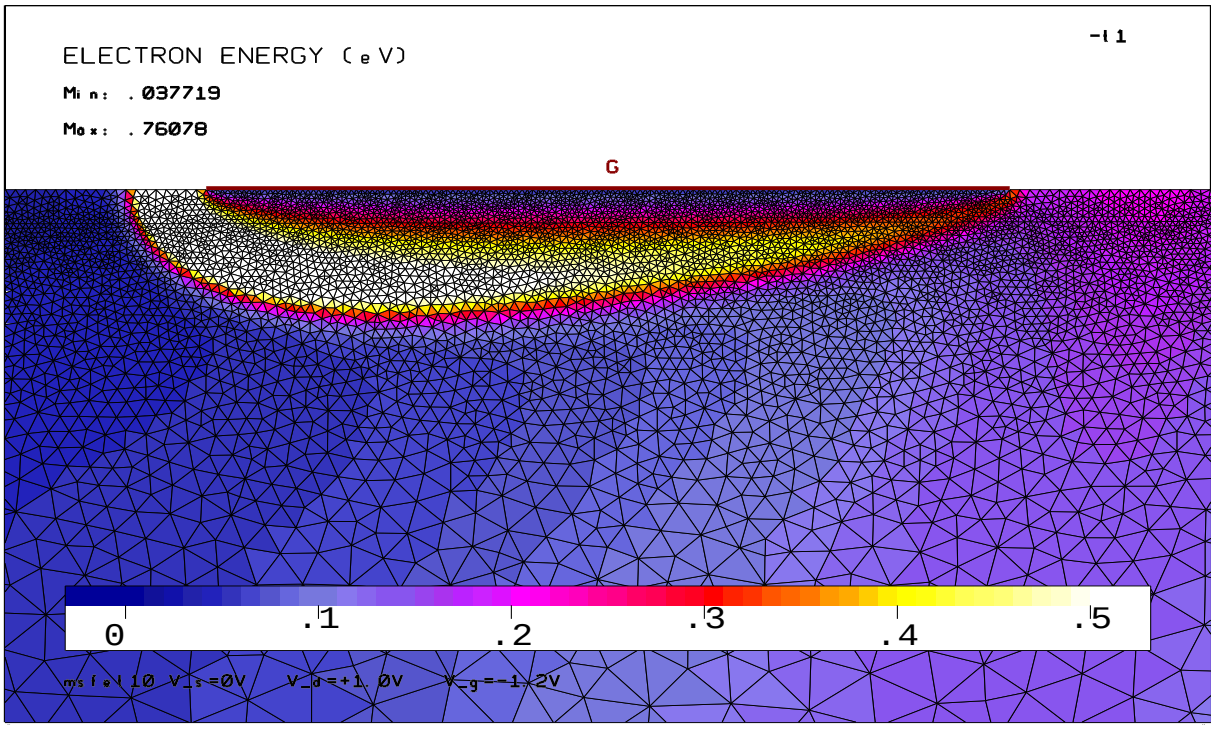

Figure 12: Distribution of electron energy for $V_G = -1.2V$ (contour plot, Zoom view).

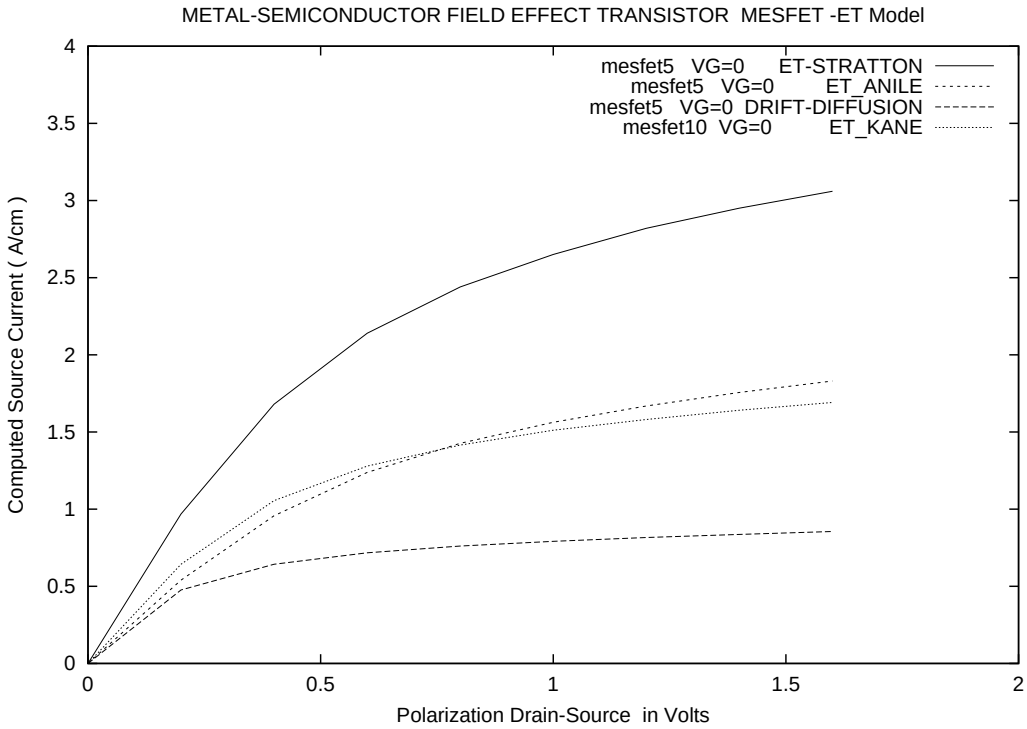

Figure 13: Characteristic curve. $I_S(V_{DS})$ at $V_G = 0$.

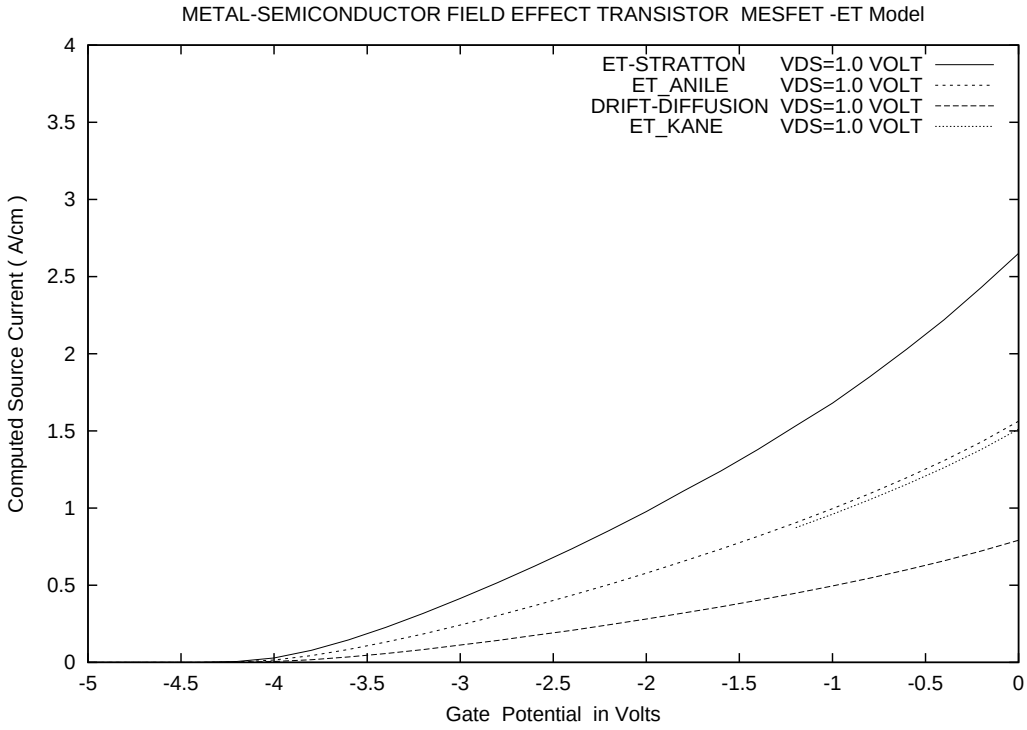

Figure 14: Characteristic curve. $I_S(V_G)$ at $V_{DS} = 1$.

The same device has been simulated in [6] by using a finite difference scheme and by considering the full hydrodynamical model based on MEP [3, 4, 5].

We denote by Γ_D that part of $\partial\Omega$, the boundary of Ω, which represents the source, gate and drain

$$\Gamma_D = \{(x,y) : y = 0.2,\ 0 \le x \le 0.1,\ 0.2 \le x \le 0.4,\ 0.5 \le x \le 0.6\}\,.$$

The other part of $\partial\Omega$ is labelled as Γ_N. The boundary conditions are assigned as follows. We have ohmic contacts in source and drain:

$$\phi = \phi_{int} + V_{app}\,, \tag{61}$$

$$\varphi_n = -V_{app}\,. \tag{62}$$

On the gate we have a Schottky contact

$$\phi = \phi_{int} + V_B + V_{app}\,, \tag{63}$$

$$\varphi_n = -V_{app}\,, \tag{64}$$

where V_B is the barrier potential modelling the Schottky contact [22]. The built in potential ϕ_{int} is the solution of

$$F(\phi_{int}) = e(n(\phi_{int}) - p(\phi_{int}) - N_D + N_A) = 0\,,$$

where the quasi-Fermi level are taken as $\varphi_n = \varphi_p = 0$. The other boundary conditions are

$$W = W_0, \quad \text{on } \Gamma_D, \tag{65}$$

$$\boldsymbol{\nu}\cdot\nabla n = 0, \quad \boldsymbol{\nu}\cdot\nabla W = 0, \quad \boldsymbol{\nu}\cdot\nabla\phi = 0, \quad i = 1,2 \quad \text{on } \Gamma_N. \tag{66}$$

Here ∇ is the bidimensional gradient operator while $\boldsymbol{\nu}$ is the unit outward normal vector to $\partial\Omega$ in the considered points. For the numerical simulation we start from the equilibrium state ($V_{app} = 0$) and after a desired bias point is reached by following a path in the space of applied potential (via potential increments). First we follow the path $V_S = 0$,$V_G = 0$ and $V_D = 0$ to 1.6 Volt by step of 0.2 Volt an after starting from the point $V_S = 0$,$V_G = 0$ and $V_D = 1$ we decrease the gate potential V_G from 0 to -5 Volt by step of 0.2 Volt. When the gate potential is sufficiently low, no ("significant") current flow from drain to source.

The results are shown in figure [5]-[14] and have to be compared with similar figures in former paper [1]. We have added here other representation of the solution (contour plots for the electrostatic potential, and electron energy).

6 Simulation of a 2D silicon MOSFET

In this section we check the validity of our energy-transport model and the efficiency of the numerical method by simulating a bidimensional metal oxide semiconductor field effect transistor (MOSFET). The shape of the device is pictured in Figure 15. The axes of reference frame are chosen parallel to the edges of the device. We take the dimensions of the silicon part of the MOSFET to be such that the numerical domain is

$$[0, 0.4] \times [0, 0.4]$$

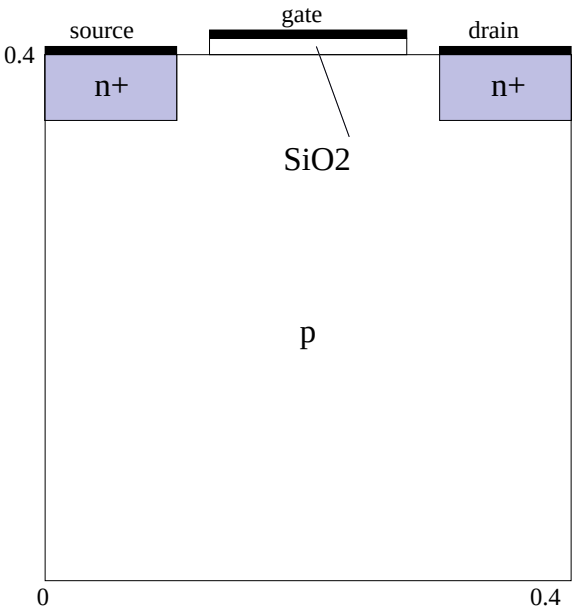

Figure 15: Schematic representation of a bidimensional MOSFET.

and at the top of the silicon part the silicon oxide domain is

$$[0.125, 0.275] \times [0.4, 0.406]$$

where the length is the micron.

The regions of high-doping n^+ are the subset

$$[0, 0.1] \times [0.35, 0.4] \cup [0.3, 0.4] \times [0.35, 0.4].$$

The contacts at the source and drain are $0.1\mu m$ wide and the contact at the gate is $0.15\mu m$ wide. The distance between the gate and the other two contacts is $0.025\mu m$. A grid of 4644 elements has been used (see figure 16): 3344 in the bulk zone, 343 in the n^+ source zone, 357 in the n^+ drain zone and 600 in the oxide zone. The doping concentration is

$$n_D(x) - n_A(x) = \begin{cases} 10^{18} cm^{-3} \text{in the } n^+ \text{ regions} \\ -10^{14} cm^{-3} \text{in the } p \text{ region} \end{cases}$$

with abrupt junctions.

We have assumed ohmic contacts on the source, drain and gate and Schottky contact on the bulk. Moreover, we have assumed homogeneous Neumann conditions on the remaining part of the boundary. In order to reach the desired bias, $V_d = 1.0$ $V_s = 0$ and $V_g = 0.5$, we first compute the equilibrium state and then the previous point is reached by continuation on applied potential. First, we go to $V_d = 1.0$ by steps of 0.1 Volt and after we go to $V_g = 0.5$ within two steps of 0.25 Volt.

We complete the table given in previous paper [1] by adding one column corresponding to the results obtained with the present approximation (Kane).

The results of the numerical integration are reported in figures (17)-(26). In each figure, we present the solution obtained via parabolic band approximation (TOP) -previous results- and the solution obtained via the Kane's band approximation (BOTTOM) -present results-.

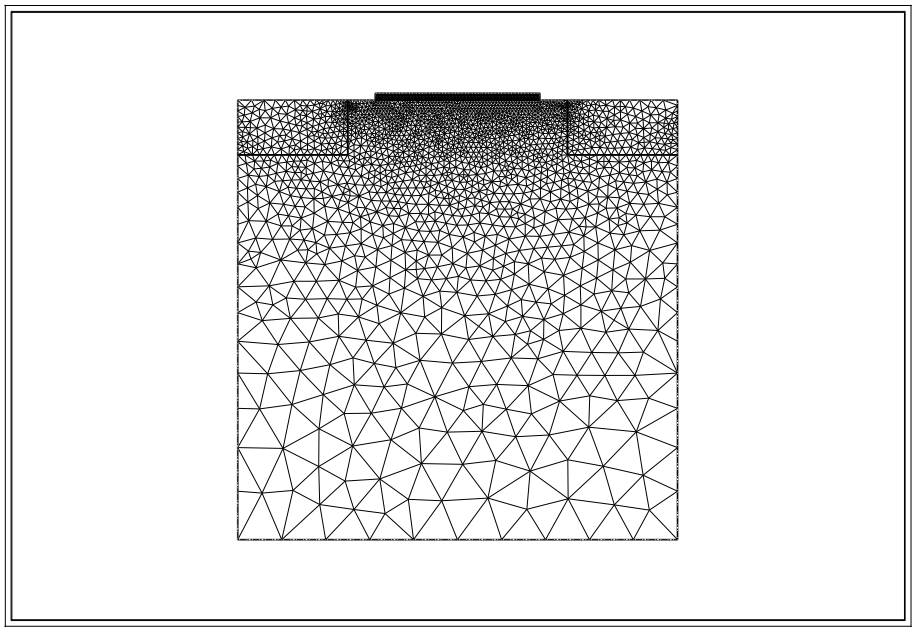

Figure 16: Mesh used for the computation.

From the figures we can see that for the Kane's approximation of energy bands (in comparison with the parabolic case)

- the electron density below the gate is higher (fig 17)
- the maximum value of the electron energy is also higher (fig 18 and fig 19)
- the electric field presents the same distribution but is also slightly higher (fig 21 and fig 22)

Conclusions and Acknowledgments

The MEP energy-transport model for charge transport in semiconductor is free of any fitting parameters and it is based on sound and consistent physical principles. The present article completes the former one [1] and shows that the simulation process can also be applied in the case of the Kane approximation of energy band. The numerical integration is based on a mixed finite element method which is very robust, guarantees accurate current conservation and is able to deal also with complex geometry.

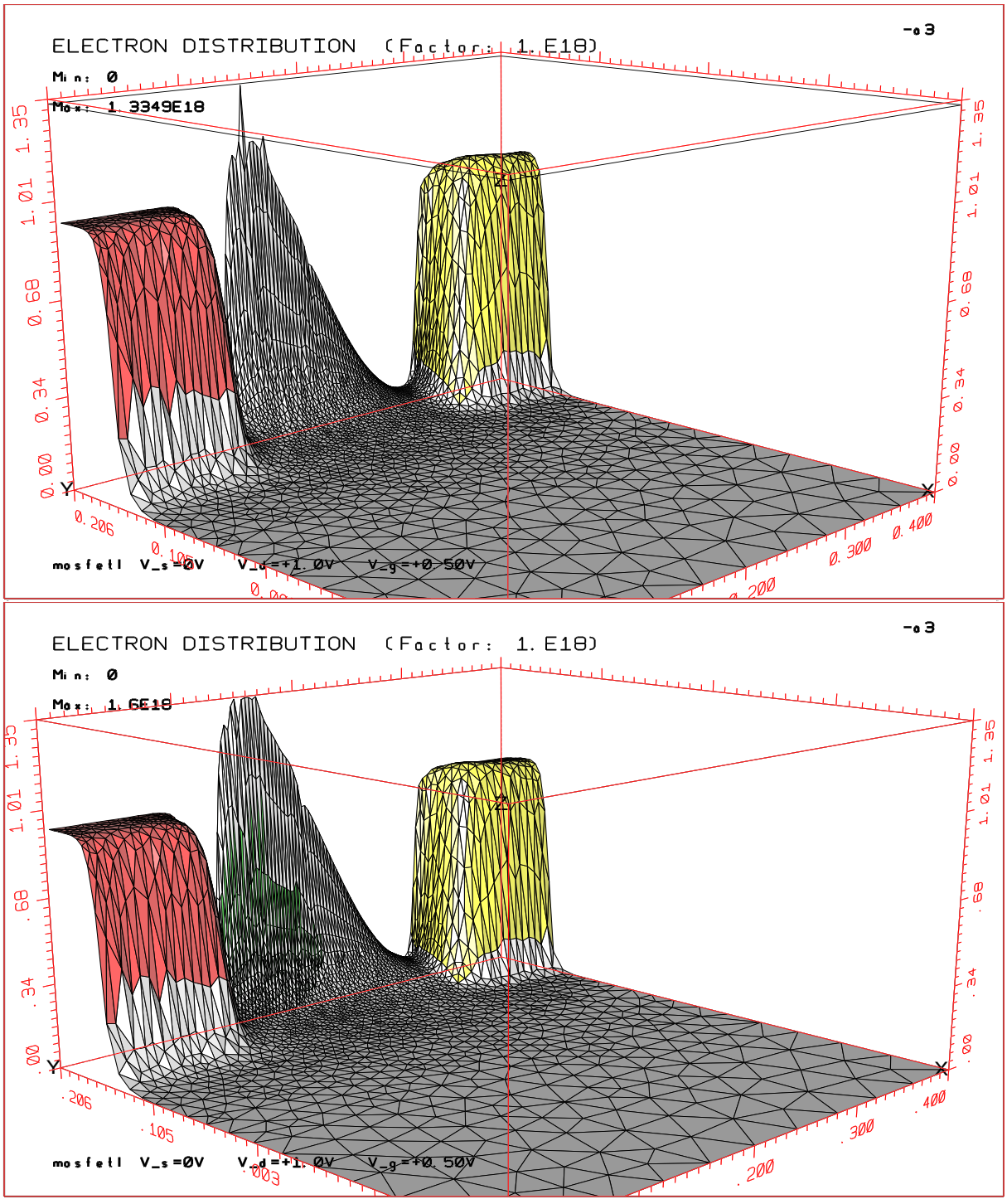

Figure 17: **Top:Parabolic band -Below: Kane's approach.** Stationary solution for the electron density in MOSFET (cm^{-3}).

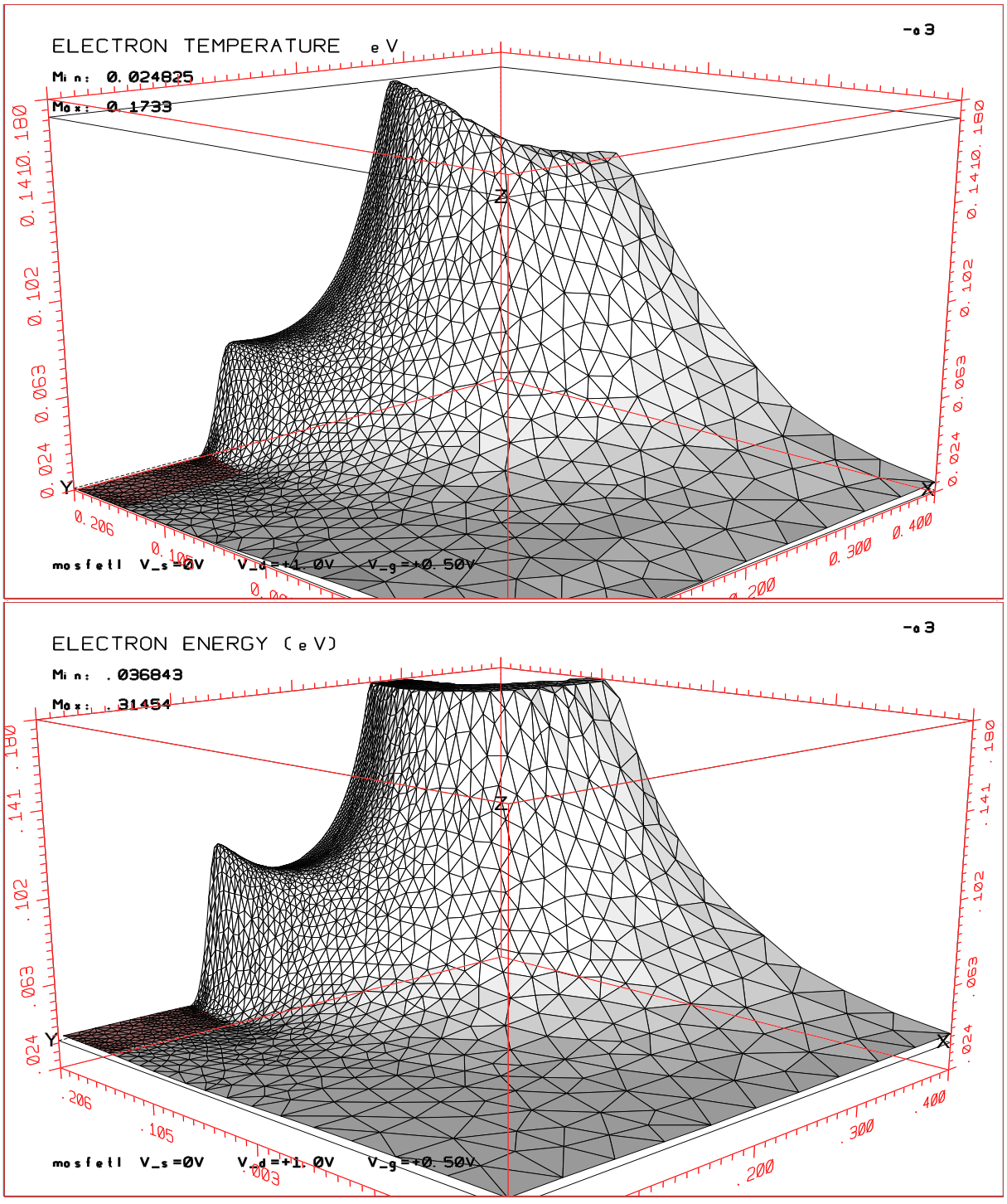

Figure 18: **Top:Parabolic band -Below: Kane's approach.** Stationary solution for the electron Energy in MOSFET (eV).

Computed Source current I_s			For the MOSFET					
			Parabolic band					Kane
Applied voltage			meshes and currents (A/cm)					
V_d	V_s	V_g	mesh 1 1198 el.	mesh 2 2521 el.	mesh 3 4644 el.	mesh 4 6094 el.	mesh 5 9796 el.	mesh 3 4644 el.
0.1	0.	0.	0.12245	0.12526	0.12722	0.12748	0.12740	0.1478
0.2	0.	0.	0.17631	0.18050	0.18278	0.18307	0.18273	0.2020
0.3	0.	0.	0.21275	0.21792	0.22038	0.22067	0.22015	0.2354
0.4	0.	0.	0.24416	0.25017	0.25282	0.25311	0.25244	0.2647
0.5	0.	0.	0.27392	0.28074	0.28358	0.28387	0.28307	0.2926
0.6	0.	0.	0.30315	0.31079	0.31382	0.31410	0.31317	0.3198
0.7	0.	0.	0.33224	0.34071	0.34393	0.34420	0.34314	0.3465
0.8	0.	0.	0.36139	0.37068	0.37412	0.37439	0.37320	0.3729
0.9	0.	0.	0.39071	0.40083	0.40450	0.40476	0.40345	0.3992
1.0	0.	0.	0.42022	0.43120	0.43509	0.43534	0.43393	0.4253
1.0	0.	0.25	1.0192	1.0406	1.0522	1.0535	1.0540	0.9782
1.0	0.	0.50	1.7228	1.7555	1.7772	1.7798	1.7835	1.5610

Table 1: **OLD RESULTS COMPLETED.** Figures presented are relatives to mesh 3.

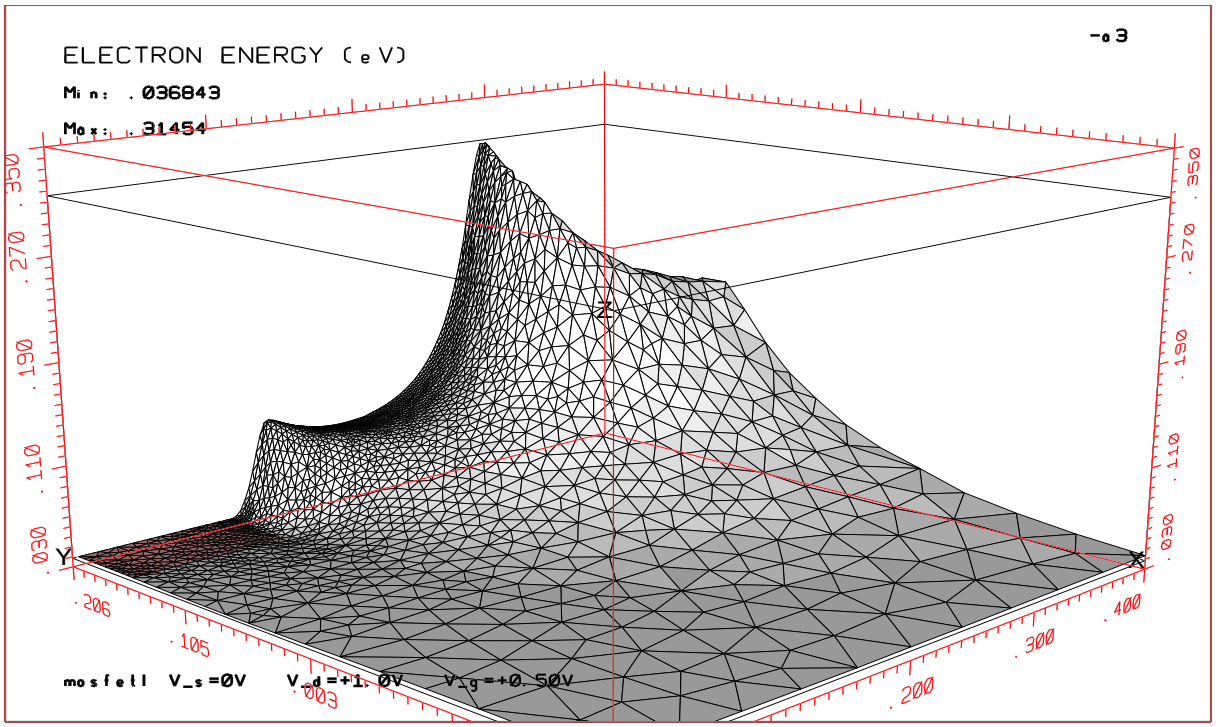

Figure 19: **Kane's approach. Adapted scale.** Stationary solution for the electron temperature in MOSFET (eV).

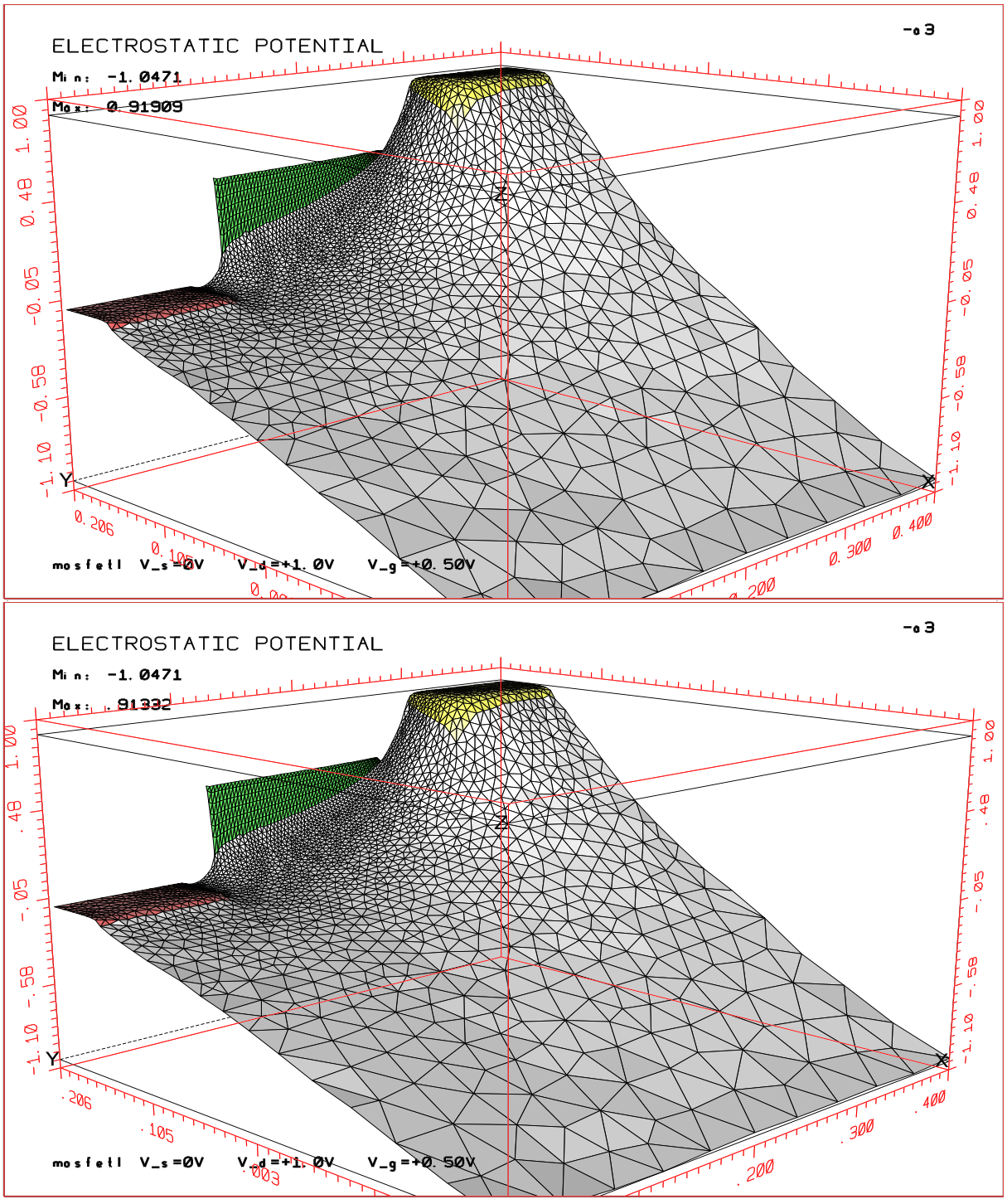

Figure 20: **Top:Parabolic band -Below: Kane's approach.** Stationary solution for the electrostatic potential in MOSFET (Volt).

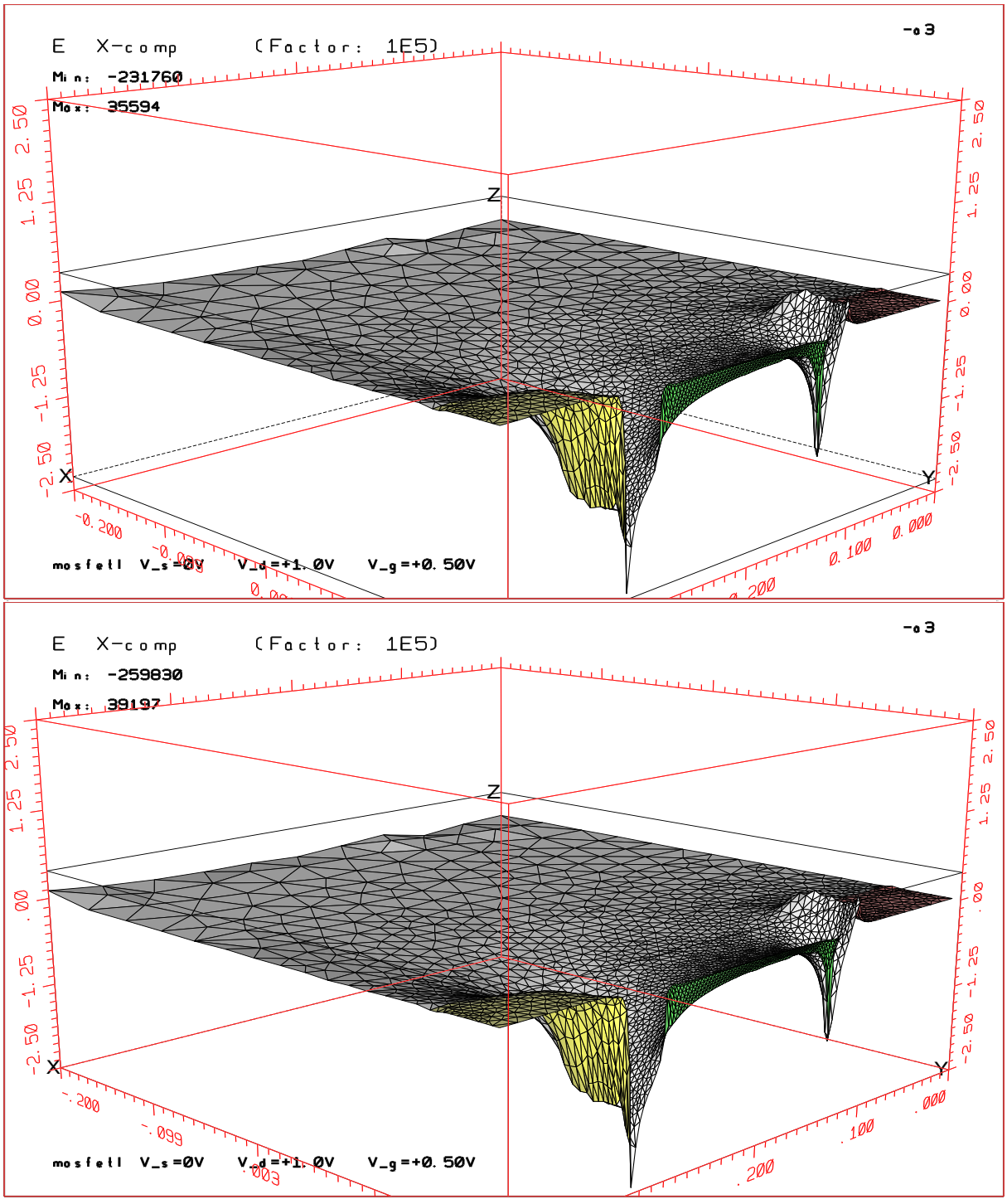

Figure 21: **Top:Parabolic band -Below: Kane's approach.** Stationary solution for the x-component of the electric field in MOSFET (Volt/cm).

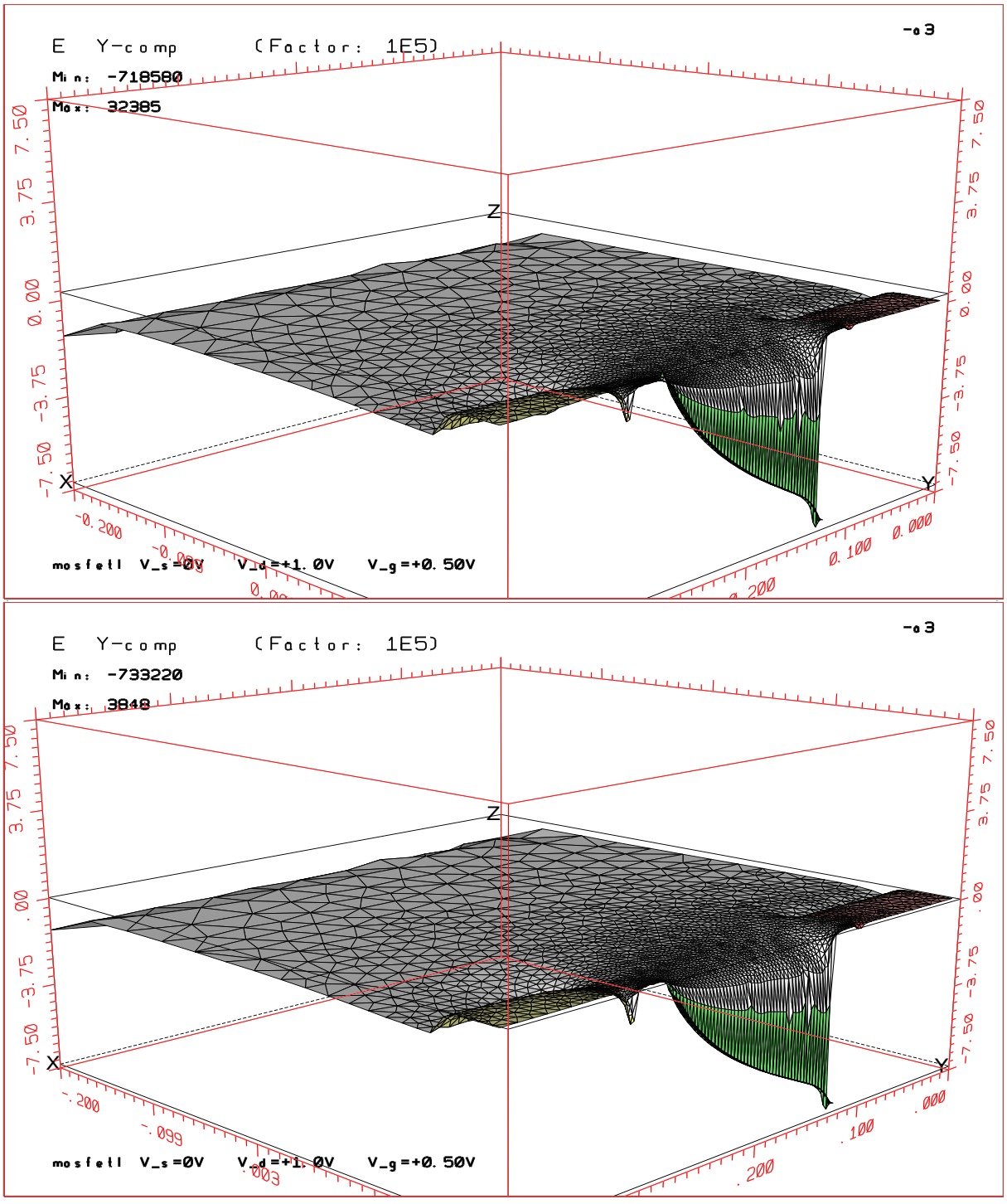

Figure 22: **Top:Parabolic band -Below: Kane's approach.** Stationary solution for the y-component of the electric field in MOSFET (Volt/cm).

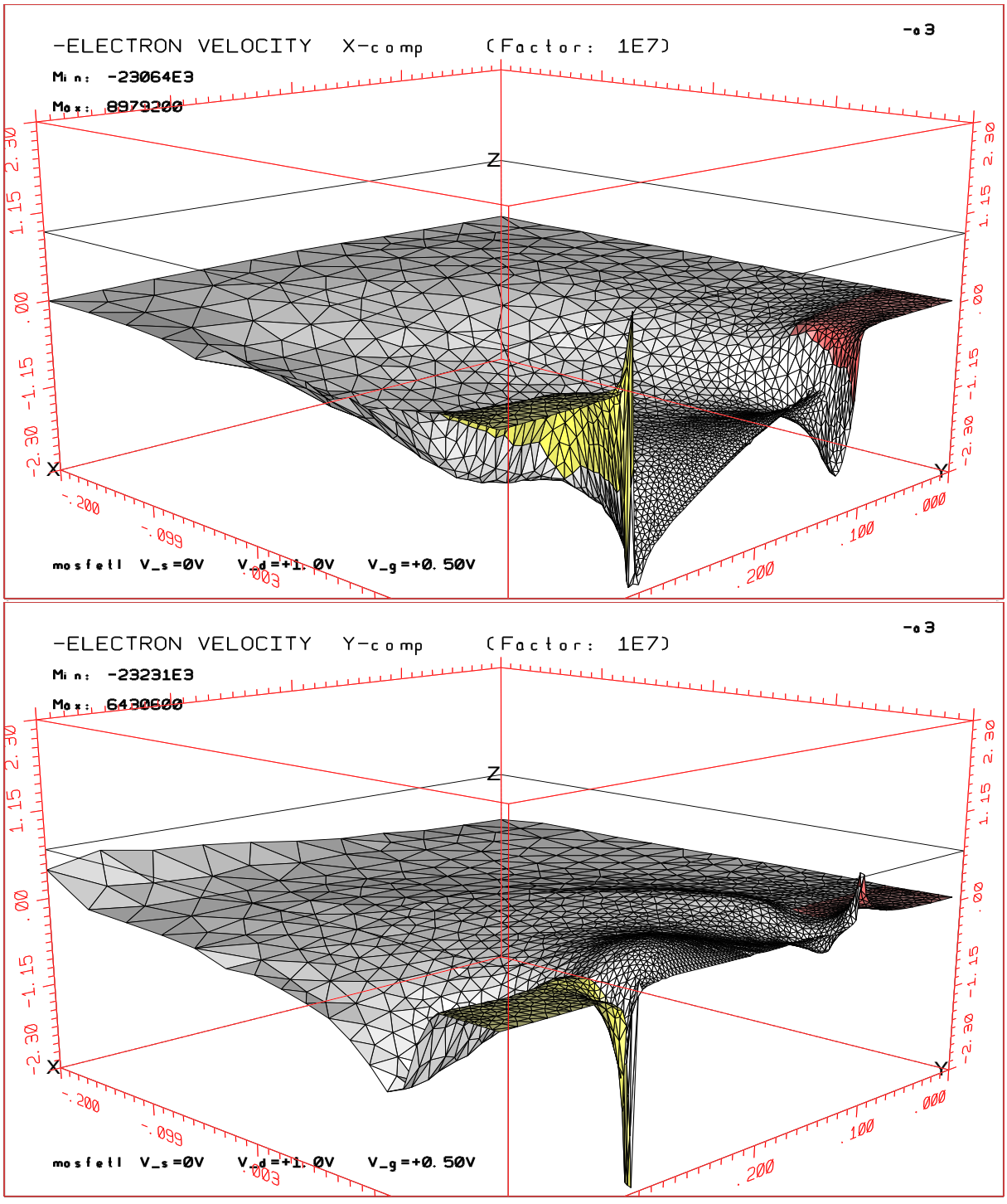

Figure 23: **Top and Below: Kane's approach.** Components of the electron velocity (cm/s).

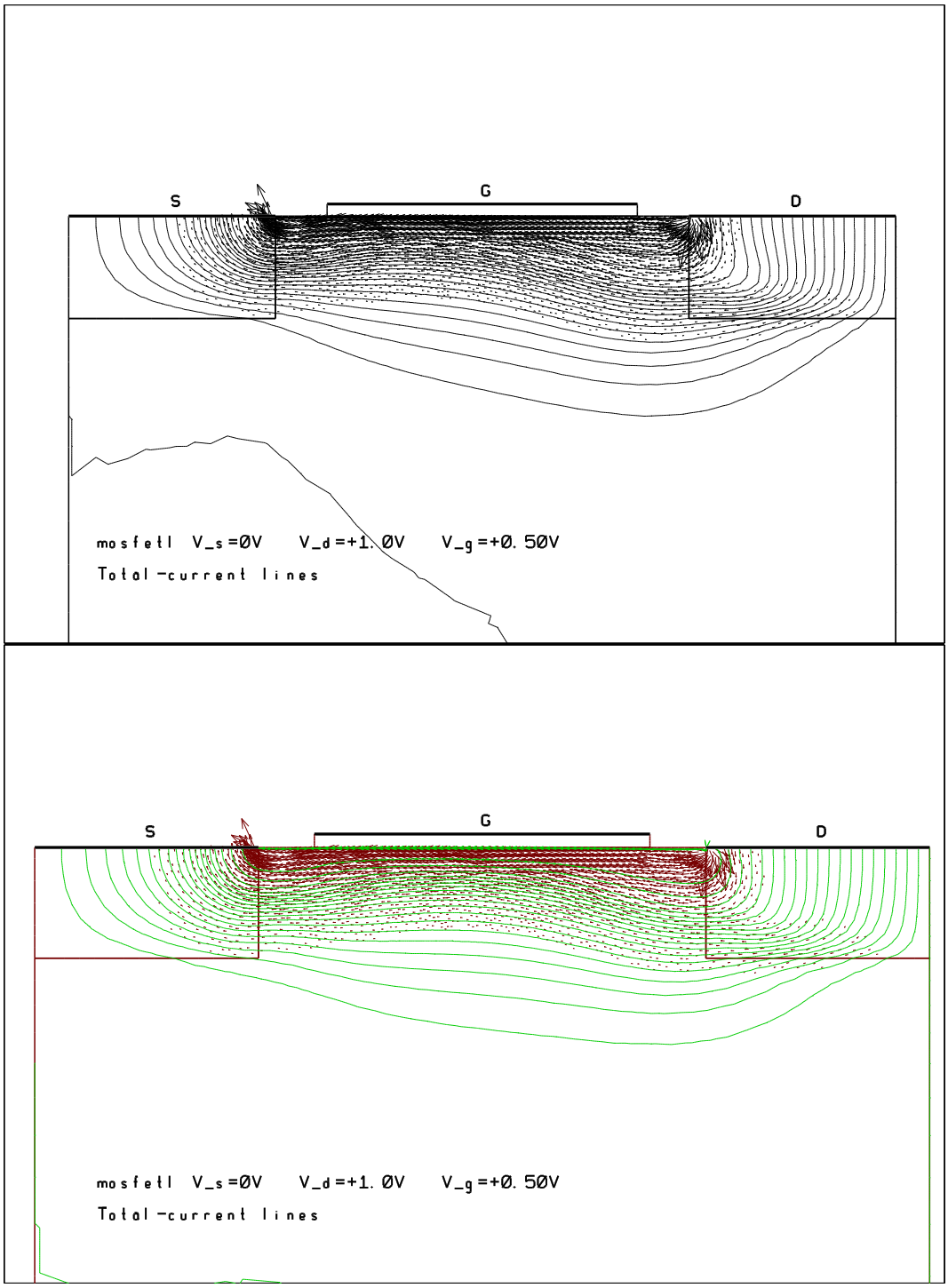

Figure 24: **Top:Parabolic band -Below: Kane's approach.** .Current lines in MOSFET for the MEP model.

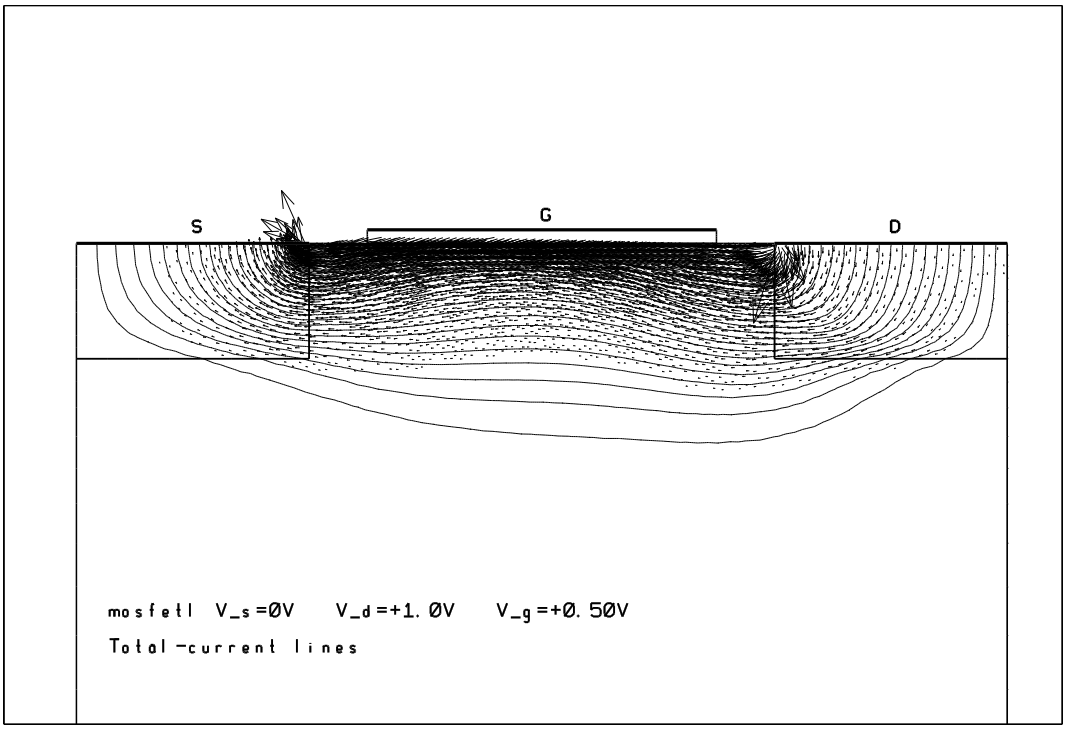

Figure 25: **Parabolic band**.Current lines in MOSFET for the Stratton model.

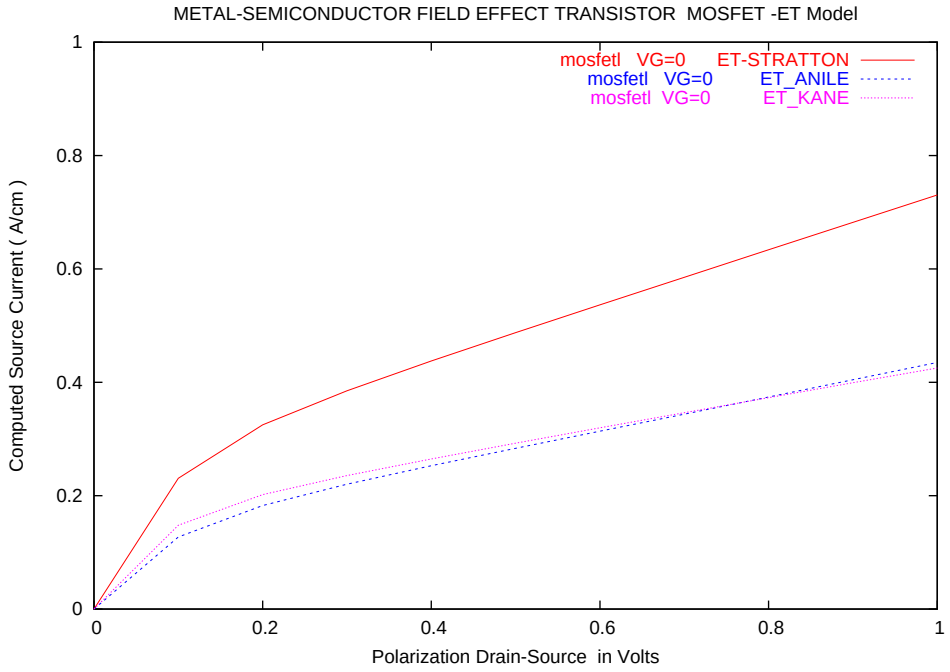

Figure 26: Characteristic curve for the MOSFET. $I_S(V_{DS})$ at $V_G = 0$.

References

[1] A.M. Anile, A. Marrocco, V. Romano, J.M. Sellier, Numerical simulation of 2D Silicon MESFET and MOSFET decsribed by the MEP based energy-transport model with a mixed finite elements scheme. Inria Research Report No 5095, January 2004.

[2] P. A. Raviart and J. M. Thomas, A mixed finite element method for 2nd order elliptic problems. In Mathematical Aspecys of Finite Element methods (I. Galligani and E. Magenes editors), Lecture Notes 606, Springer-Verlag 1977, pp. 292-375.

[3] A.M. Anile, V.Romano. Non parabolic band transport in semiconductors: closure of the moment equations, Continuum Mech. Thermodyn. (1999) 11:307-325, Springer-Verlag 1999.

[4] V.Romano. Non parabolic band transport in semiconductors: closure of the production terms in the moment equations, Continuum Mech. Thermodyn. (2000) 12:31-51, Springer-Verlag 2000.

[5] V.Romano. Non-parabolic band hydrodynamical model for silicon semiconductors and simulation of electron devices, Math. Meth. Appl. Sci. (2001), 24:439-471, John Wiley and Sons, Ltd. 2001.

[6] V.Romano. 2D simulation of a silicon MESFET with a nonparabolic hydrodynamical model based on the maximum entropy principle, J. Comp. Phys. (2002) 176: 70-92.

[7] A.Schenk. *Advanced Physical Models for Silicon Device Simulation.* Springer Wien New York.

[8] Ph. Montarnal. Modèles de transport d'énergie des semi-conducteurs, études asymptotiques et résolution par éléments finis mixtes. Thèse de doctorat, Université Paris VI, oct. 1997.

[9] A. Marrocco, Ph. Montarnal. Simulation des modèles energy-transport à l'aide des éléments finis mixtes. C.R. Acad. Sci. Paris, Vol.323, Serie I, 535-541, 1996.

[10] Ben Abdallah, N., Degond, P., and Genieys, S., 'An energy-transport model for semiconductors derived from the Boltzmann equation', *J. Stat. Phys.* **84** (1996) 205-231.

[11] Ben Abdallah, N., and Degond, P., 'On a hierarchy of macroscopic models for semiconductors', *J. Math. Phys.* **37** (1996) 3306–3333.

[12] D. Chen, E. C. Kan, U. Ravaioli, C-W. Shu, R. Dutton, *An improved energy-transport model including nonparabolicity and non-maxwellian distribution effects*, IEEE on Electron Device Letters, 13:26–28 (1992).

[13] E. Lyumkis, B. Polsky, A. Shir and P. Visocky, *Transient semiconductor device simulation including energy balance equation*, Compel 11: 311–325 (1992).

[14] R. Stratton, *Diffusion of hot and cold electrons in semiconductor barriers*, Phys. Rev., 126 (1962), pp. 2002–2014.

[15] Ashcroft N W and Mermin N D (1976), Solid State Physics, Philadelphia, Sounders College Publishing International Edition

[16] S. R. de Groot and P. Mazur, *Non Equilibrium Thermodynamics*, (Dover Publications Inc.,), New York, (1985)

[17] G. Mascali and V. Romano, Si and GaAs mobility derived from the hydrodynamic model of semiconductors based on the maximum entropy principle, preprint 2003.

[18] F. Brezzi, M. Fortin. Mixed and Hybrid Finite Element Methods. Springer Series in Computational Mathematics 15, Springer-Verlag (1991).

[19] R. Glowinski, P. Le Tallec. Augmented Lagrangian and Operator Splitting Methods in Nonlinear Mechanics, SIAM, Studies in Applied Mathematics, Philadelphia, 1989.

[20] Ch. Faure, Y. Papegay. Odyssée user's guide, version 1.7. Rap. Tech., R.T.0224., Sept.1998.

[21] J. W. Jerome and C-W. Shu, *Energy models for one-carrier transport in semiconductor devices*, in *Semiconductors part II*, The IMA volumes in Mathematics and its Applications, N. M. Coughran, J. Cole, P. Lloyd, J. K. White editors (1994), pp. 185–207.

[22] S. Selberherr, *Analysis and simulation of semiconductor devices*, Wien - New York, Springer-Verlag, 1984.

Unité de recherche INRIA Rocquencourt
Domaine de Voluceau - Rocquencourt - BP 105 - 78153 Le Chesnay Cedex (France)

Unité de recherche INRIA Futurs : Parc Club Orsay Université - ZAC des Vignes
4, rue Jacques Monod - 91893 ORSAY Cedex (France)
Unité de recherche INRIA Lorraine : LORIA, Technopôle de Nancy-Brabois - Campus scientifique
615, rue du Jardin Botanique - BP 101 - 54602 Villers-lès-Nancy Cedex (France)
Unité de recherche INRIA Rennes : IRISA, Campus universitaire de Beaulieu - 35042 Rennes Cedex (France)
Unité de recherche INRIA Rhône-Alpes : 655, avenue de l'Europe - 38334 Montbonnot Saint-Ismier (France)
Unité de recherche INRIA Sophia Antipolis : 2004, route des Lucioles - BP 93 - 06902 Sophia Antipolis Cedex (France)

Éditeur
INRIA - Domaine de Voluceau - Rocquencourt, BP 105 - 78153 Le Chesnay Cedex (France)
http://www.inria.fr
ISSN 0249-6399